Electronic Supplementary Material (ESI) for Chemical Society Reviews.
This journal is © The Royal Society of Chemistry 2017

Supplementary Information

Recent Advances in Nanomaterials for Water Protection and Monitoring

Rasel Das,[a,*] Chad D. Vecitis,[b] Agnes Schulze,[a] Bin Cao,[c] Ahmad Fauzi Ismail,[d] Xianbo Lu,[e] Jiping Chen[e] and Seeram Ramakrishna[f,*]

[a]Leibniz Institute of Surface Modificatioponytailn, Permoserstr 15, D-04318 Leipzig, Germany.

[b]School of Engineering and Applied Sciences, Harvard University, Cambridge, Massachusetts 02138, United States.

[c]School of Civil and Environmental Engineering, Nanyang Technological University, Singapore.

[d]Advanced Membrane Technology Research Center, Universiti Teknologi Malaysia, 81310 Johor, Malaysia.

[e]CAS Key Laboratory of Separation Science for Analytical Chemistry, Dalian Institute of Chemical Physics, Dalian 116023, China.

[f]Center for Nanofibers and Nanotechnology, Department of Mechanical Engineering, National University of Singapore, 117584, Singapore.

---

[*] **Corresponding Author**

E-mail: raseldas@daad-alumni.de/rasel.das@iom.leipzig.de, (R.Das), Tel: + +49 (0)341 235 – 3147; Fax**:** +49 (0)341 235 – 2584, seeram@nus.edu.sg, (S. Ramakrishna).

1. Current and Potential Selected Nanomaterials for Water Treatments

1.1 Carbon Nanostructures

The reactive carbon atoms can form direct covalent bonds with other carbons elements through different hybridization states (sp, sp^2, sp^3) that result in wide range of carbon nanostructures such as 0D fullerene, 1D CNT and CNF, 2D GFM and 3D carbon superstructures.[1] Due to their different sizes and crystallinity, the properties of carbon nanostructures are completely different;[2] suggesting their potential applications in wastewater treatment would be varied significantly. Based on size variations (from bulk to nano state), the carbon nanostructures would have different surface energies[3]; which ultimately determine their stiffness and adhesion energy. An understanding of these energies is critical in terms of knowing the aggregation and dispersibility of the carbon nanostructures in water. However, efficacious hybrid NMs-based technology (e.g., carbon aerogels, thin films, etc.) for water purification can be build up by merging 0D, 1D, and 2D carbon nanostructures. CNTs are found popular in wastewater treatment than the other carbon nanostructures may be because of their well-defined pore structures and surface functionality that facilitate specific surface reactions.

1.1.1 Fullerene

Fullerenes commonly known as buckyballs are classified as an intermediate between long spherical organic molecule and sp^2 and sp^3 hybridized nanoallotrope. Initially observed in 1985 as the predicted C_{60} molecule consisting of 60 carbon atoms.[4, 5] Subsequently C_{20}, C_{70}, C_{80}, C_{94} and similar structures have been discovered, but C_{60} has been the most extensively studied to date. Fullerene is synthesized via Kratschmer-Huffman AD[6] and chemical synthesis methods.[7] Fullerene carbon atoms arrange in 12 pentagonal (perfect structure) and 20 hexagons to build a truncated icosahedra (spherical) structure, i.e., a fullerene (C_{60}) consisting of $20 + 2n$ carbon atoms will have n hexagons. The external diameter of a fullerene molecule is 0.71 nm.[2] Fullerenes are chemically stable and can be easily functionalized by wet chemical agents. Fullerene is photocatalytically active in solar spectrum, but may not be beneficial for adsorption due to low SSA (5 m^2/g)[8]. BCC-research proclaims that the fullerene market would exceed US \$4.7 billion by 2016, but most of its will be used in energy sector.[9] The price of C_{60} was US \$0.33/kg in 2010[10] which is currently about US \$4536/kg[11] with the high cost due to complicated purification strategies (e.g., C_{60} needs to be isolated from other fullerene molecules). In order to use fullerene for bulk water treatment; the cost of the material should not exceed US \$45/kg.

1.1.2 Carbon Nanotube

CNT is one of the quintessential and fascinating NMs of the 21st century. Although initially a fortuitous discovery,[12] Iijima (1991)[13] later atomically defined the material. Among CNT synthesis methods, chemical vapor deposition (CVD) is more popular than arc discharge (AD) and laser ablation (LA) for CNT production because of its low cost, simple set-up that utilizes cheap catalysts (Fe, Ni, Co etc.) and carbon sources (coal, charcoal, asphalt etc.).[14] CNT is composed of a hexagonal array of sp^2 carbon atoms (graphite sheet) rolled to in a cylindrical tube-like shape with one end initially capped by a fullerene-like tip that is easily oxidatively opened.[15] CNT can be categorized as either single-walled carbon nanotube (SWCNT) consisting of a single graphene sheet[16] where 1/3 are metallic and 2/3 are semiconductive depending on chirality. On the other hand, multi-walled carbon nanotube (MWCNT) composed of 3 or more concentric multiple graphite sheets where all are conductive.[13] The CNT length can be in μm range, and the SWCNT diameter (0.2-2.0 nm) and the MWCNT diameter (2-100 nm). CNT have superior properties such as high mechanical (elasticity: 1 TPa and tensile strength: 50-500 GPa), thermal stability (>700°C), and electrical conductivity (3000-3500 W m^{-1} K^{-1}).[17-19] In regard to water treatment, CNT have been used as adsorbents, photo- and biocatalysts supports, antimicrobial surface, membranes, and sensors.[20, 21] Commercial CNT potential can be estimated from its market production value of US $37 million (SWCNT) and US $630 million (MWCNT) and is expected to reach US $1.1 billion by 2016.[22] Nearly 750 metric tons of CNT were utilized over the past few years for energy and environmental applications and continues to increase.[23] Current prices of SWCNT and MWCNT are US $25-300 and US $0.10-25/g, respectively.[24] While MWCNT may not have some of the superior SWCNT individual properties, the significant cost reduction would more than compensate for performance reduction while still providing an enhanced material. It has been calculated that average costs of SWCNT is US $1.26 and 2.2/g for organic and inorganic pollutants removal, respectively. On the contrary, MWCNT will decrease cost to US $0.22 and 0.57/g for organic and inorganic pollutant removal, respectively.[24] Here it is important to note that since there is no actual cost per mass of pollutant removed has been reported, Adeleye et al.[24] measured some rough cost using a snowball-type approach by taking information from existing studies. Cost was determined using the cost to treat a volume of wastewater with a given engineered NMs-based technology relative to the typical influent concentration for a given pollutant. The cost of NMs for pollutant removal that we mention below has been determined from Adeleye et al.[24] in order to show a rough idea of their commercial feasibility, but one should not forget that cost of such technology depends on their reusability, pollutants concentration, types, wastewater matrix etc.

1.1.3 Carbon Nanofiber

CNF is a sp^2-based carbon allotrope consisting of noncontinuous graphite fiber. CNF synthesized by using catalytic CVD and catalytic-plasma-enhanced CVD methods.[25] Alternatively, electrospinning is a common method to produce continuous CNF[26, 27]due to simple methodology.[45] CNF have an average diameter of 50-200 nm and an aspect ratio ≥ 100. CNF graphene layer geometry can be categorized into platelet, herringbone/fishbone and ribbon, or tubular perpendicular alignment, tilted and parallel to the fiber axis, respectively (Fig. S1 (a, b and c)). Alternative CNF family members are stacked-cup/cone-stacked and cone-helix consisting of truncated cones with helix architectures resulting large hollow cores (Fig. S1 (d)).[25]

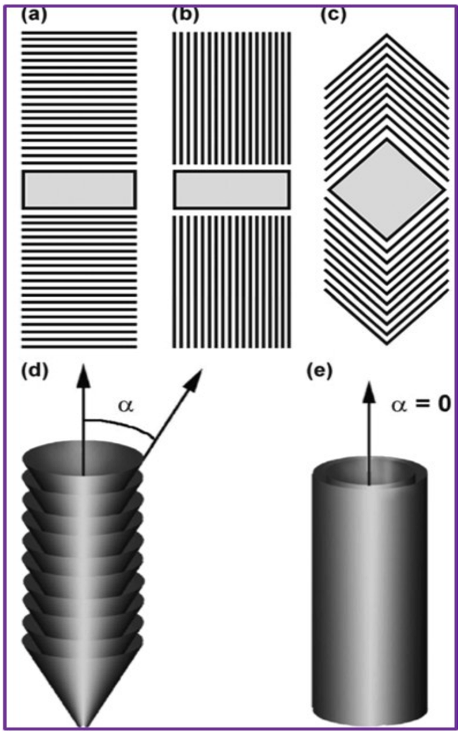

Fig. S1. Examples of CNF: (a) platelet, (b) ribbon and (c) herringbone. Structural difference between the (d) CNF and (e) CNT. Panels a, b and c reprinted with permission from ref.[2] Copyright 2014 American Chemical Society; and panels d and e reprinted with permission from ref.[28] Copyright 2005 American Institute of Physics.

CNF cone-helix lack of hollow core which is viewed as a main difference from CNT. If $\alpha = 0$, a continuous CNT structure will be restored (Fig. S1 (e)). CNF with cone and tilted-graphene sheet motifs can be characterized when $\alpha > 0$. Thence the angle determines the physicochemical properties of CNF. In general, CNF has almost similar physicochemical properties such as high mechanical, electrical, and thermal properties to CNT. CNF has been studied in detail as an adsorbent for water pollutants, it uses for catalysis, separation, and advanced redox has yet to be widely studied. Pyrograf Products Inc. reports nearly 70,000 pounds of CNF have been produced in recent years with the market price ranging from US \$200 to 1000/kg.[29]

1.1.4 Graphene Family Members

Pristine graphene (PG) is single atom thick sp^2 hybridized carbon in a 2D honeycomb lattice and is the fundamental building block of graphite. Boehm et al.[30] first experimentally identified PG in 1962, and a complete characterization was eventually completed by Novoselov et al.[31] in 2004. PG is synthesized by exfoliation of graphite in presence of specific organic solvents under ultrasonications.[32] Based on the number of layers presence, PG classifies as single, a few- (2-5), multi- (2-10) graphene monolayer. Graphene layers >10, but <100 nm in thickness or lateral dimensions constitute a graphite nanoplate/sheet. Two alternative GFM are graphene oxide (GO) and reduced GO (rGO) synthesized by the oxidative exfoliation of graphite[33-36] and reduction of the GO, respectively.[36-38] Graphene quantum dot (GQD) is a recently identified GFM.[39] GFM have physicochemical properties, e.g., (Young's modulus: 1 TPa, intrinsic strength: 130 GPa, electronic mobility: 2.5×10^5 $cm^2 V^{-1}s^{-1}$ and thermal conductivity: >3000 WmK^{-1}).[40] GFMs have been examined as adsorbents, photo- and biocatalysts supports, membranes, antimicrobial materials and sensors. Several market research services suggest future GFM market prices of US \$126 million (Lux research), US \$1 billion (Graphenea), and US \$390 (IDTechEx's) by 2020, 2022, and 2024, respectively.[41] Current GFM prices range from US \$2.50 to 1000/g. About 1 mg of organic pollutants removal from aqueous solution will cost US \$1.77 and US \$5.23 using GO and rGO, respectively;[24] suggesting a high expensive option than the CNT and CNF.

1.2 Metal and Metal Oxide Nanoparticles

Noble metal[42] and metal oxide[43-45] NPs have large surface area, but much lesser than the carbon nanostructures; and can be easily functionalized with chemical groups to increase affinity for target pollutants to be removed. In the bulk state, most of the metal particles have shown low reactivity. Decreasing the metals size at nanoscale helps to expose more surface reactive atoms and the functional groups which have been located at distal places will come-up closer for enhanced chemical reactivity. But because of their high reactivity, the NP undergoes self-oxidation processes and become extremely unstable. Therefore, they have been widely studied as a component of nanocomposites rather than isolated counterpart.

1.2.1 Nanoscale Zero-Valent Iron

Nanoscale zero-valent iron (nZVI) can be synthesized using top down methods (e.g., abrasion, grinding, milling, and lithography) and bottom up approaches (e.g., chemical reduction, ultrasound, and electrochemistry).[46] It has zero valent metallic iron core surrounded by iron oxide surface layer. Most of the synthesized nZVI has diameter in the range of 10-100 nm, which can be controlled via synthesis method selected. nZVI is widely used as a building block permeable reactive barriers for *in-situ* ground water remediation, particularly; perchlorates, arsenic (As) and chlorinated hydrocarbons.[47] NANOFER 25S is a commercial nZVI-based technology, which shows a high reactivity with a large scale of pollutants and very low degree of agglomeration. Worldwide >50 nZVI pilot projects[48] have been implemented suggesting that nZVI is effective for environmental clean-up (adsorption, degradation, and precipitation) because of its reactivity, abundance, and low cost (US $3.75/kg ARS Technologies Inc., New Jersey, USA). It costs only US $0.00077/mg of As removal from water.

1.2.2 Nano Silver

Pristine Ag NP is a crystalline form of metal Ag (0) particle having at least one dimension in between 1 and 100 nm. They are obtained by wet chemistry, ion implantation and biogenic processes.[49] Ag NP produced with a number of morphologies such as spherical, rod, prismatic, and cubic with the size and shape controlling reactivity. For example, decreasing Ag NP size increases antibacterial activity[50] because of greater SSA and Ag toxicity as function of Ag^+ dissolution. Ag NP are high thermal and electrical conductive, and surface enhanced Raman scattering (SERS) making them versatile for application field.[49] Ag can be used as either individual NP for water disinfection or it has potential to work as a component of other nanocomposites used for adsorption, catalysis, separation, and sensors. The commercial price of Ag NP is US $ <10/g, and a cartridge having 120 g of Ag NP-based antimicrobial composite can provide 3700 L of drinking water for a 5 member family. An expense for this has been calculated only US $2 for media replacement, sediment pre-filter, plastic assembly, and cartridge packing.[24] It has been used in household water filter for a longer period of time.[51]

1.2.3 Nano Titanium Dioxide

Titanium dioxide (TiO_2) is a well-known transition metal oxide semiconductor. Nanoscale TiO_2 can be provided in a number of morphologies such as NP, nanotubes, and nanorods. Based on their synthetic method (e.g., sol-gel, hydrothermal, solvothermal etc.) and conditions, one can scrutinize size-dependent properties such as surface reactivity, mechanical, optical, and electrical characteristics that are a function of surface and bulk crystallinity. TiO_2 NP exists as three major polymorphs e.g., rutile, anatase, and brookite, that all have octahedral coordination. Rutile is more thermodynamically stable than anatase and brookite. Anatase is photo-active in the solar spectrum, and thus has been studied widely for water treatment. TiO_2 abundance and stability promote industrial use, e.g., paints, papers, pigments, antimicrobial coatings, and environmental application.[52] The US alone (Altair and DuPont)[53] produced 1.5 Mt bulk TiO_2. Realizing this market demand, only the US produces 1 Mt bulk TiO_2 in 2016 where nearly 10% being TiO_2 NP and within 10 years >90% is projected to be nano. Current price of TiO_2 NP ranges from 0.03 to 1.21 USD, and the treatment cost is between US $0.50 and 1.0/g of water pollutants removal using engineered TiO_2.[24] Graver Technologies and DOW international companies commercialized MetSorb and ADSORBSIA™, respectively which utilize TiO_2 NP as convenient and cost effective options for removing As from drinking water. In addition, some commercial TiO_2 photocatalysts e.g., Nippon Aerosil P-25,[54] Kronos,[55] Tayca TKP101, TKP102, and Evonik P25 are available in the market. Since photocatalysts are not degraded in the production of oxidizing radicals, their recrudescence and reusability would be a possible chance for their wide applications in water treatment.

1.2.4 Nano Iron Oxide

Iron oxide NP is produced in the forms of magnetite (Fe_3O_4) and its oxidized form maghemite (γ-Fe_2O_3) and both forms are magnetic. They can be synthesized by co-precipitation, thermal decomposition, microemulsion, and flame pyrolysis.[56] Ferrite displays superparamagnetic behavior when their sizes <128 nm,[56] and shows magnetic behavior (saturation, Ms: 90 emu/g)[57] when an external magnetic field is applied. Iron oxide NPs have been widely used as supports for other NPs and polymers to magnetically recover adsorbents and catalysts in both lab and field experiments. The price of Fe_3O_4 NP was US $0.44/g in 2010, and is currently significantly reduced at bulk levels.[10] ArsenXnp (SolmeteX Inc., Philadelphia, PA, USA)[58] is a commercially available magnetic NPs based adsorbent for As removal and can be easily regenerated. In summary, a magnetic NP has all essential properties which should be present to be an ideal NP for wastewater treatment. For example, it has surface at which contaminants attached, a shell that provides stability and protects from oxidation and a core that facilitates their recovery.

1.2.5 Nano Silicon Dioxide

Silicon dioxide (SiO_2) is naturally abundant and convenient NP (5-25 nm) for water treatment. SiO_2 is produced by sol-gel process, reverse microemulsion, and flame synthesis.[59] SiO_2 NP having diameter (<5 nm) will have greatly increased surface silanol groups (≡Si-OH),[60] which can be used to graft of foreign organofunctional groups or anchor metal ions to the surface (≡Si-OH) groups. The low production cost, high accessibility, non-toxicity, and environmental safety have resulted in SiO_2 NP being used in a number of water treatment sectors such as adsorptions, catalysis and membranes. SiO_2 NP market was US $1.62 billion in 2014 due to its usage in a variety of commercial products.[61] The cost of SiO_2 NP for water treatment is difficult to estimate, since SiO_2 NP are commonly used as composite materials. In summary, because of its diverse availability and specificity, SiO_2 NP can be implemented in continious manner and target specific pollutant removal, respectively.

1.2.6 Nano Zinc Oxide

Nanoscale zinc oxide (ZnO) have typical diameters of 20-45 nm and can be produced in a range of morphologies e.g., nanoflowers, nanorods, nanowires, tetrapods, NPs, and spheres, by a number of methods such as hydrothermal, sol-gel, CVD, laser ablation, ultrasound, and anodization.[62] ZnO has a tetrahedral crystal structure with a hexagonal unit cell appears as noncentro-symmetric structure.[63] ZnO NPs are transparent and have a high electron mobility, and ambient luminescence. Water purification have evaluated the use of ZnO NPs as adsorbent, photocatalyst, and disinfectant. Current global market demand of ZnO NP is 30,000 t/year.[64] US-Research International Inc. determines an average cost of pure ZnO NP (80-200 nm) is US $0.46/g which can be used as a less expensive alternative to Ag NP for water disinfection, if the efficiency of both are same in actions. Therefore, if highly reactive ZnO NP able to be used at appropriate environment espicially antimicrobial and photocatalysis will become one of the most promising wastewater treatment technologies due to its flexible and manifold implementation and easy scalability.

1.2.7 Nano Aluminum Oxide

Aluminum oxide (Al_2O_3) NP typically consists of α, γ, δ, and θ phases among which α is thermodynamically stable and can be synthesized by sol-gel, hydrothermal, ball milling, pyrolysis, and laser ablation.[65] Al_2O_3 NP has been widely used because of its enhanced properties, e.g., high stability and hardness, electrically insulating and transparent. Al_2O_3 NP is popular in the fields of adsorption, catalysis, antimicrobial as well as additive to ceramic and polymer membranes. Current commercial price of Al_2O_3 NP (<50 nm) is US \$3.7/g, which is relatively expensive as compared to other NPs (e.g., nZVI, TiO_2) for water treatment. Nevertheless, α-Al_2O_3 has been commercially used as a component of ceramic composite membrane. NanoCeram® (Argonide Corporation, Sanford, FL, USA) is a filter media fabricated using Al_2O_3 nanofibers and cellulose and effective adsorptions of organic dirt, bacteria, viruses, and proteins. To conclude, compared with many NPs, Al_2O_3 would be a first priority NP for scientists for developing wastewater treatment technology especially catalysis and membrane where stability is a major concern.

1.2.8 Nano Ceramic

Ceramic NPs are composed of inorganics such as hydroxyapatite, zirconia (ZrO_2) and others[66] that are sythesized by sol-gel, sintering, and laser ablation. Bulk cerramic is brittle and break upon impact, whereas cermaic NP is a very light, strong, flexible, durable, extremly heat, and chemically stable.[67] Ceramic NPs have been widely studied for membrane separation, however, ceramic membranes cost 5-10 times higher than classical polymer membranes,[68] which may be offset by incraesed recyclability of the highly stable ceramic membrane. Commercial ceramic membranes are CeraMem® and Membralox® which have been used as point-of-use (POU) devices for water purification. Therefore, ceramic based wastewater treatment technology would have high separation characteristics and long working life even in harsh wastewater effluents.

1.2.9 Nano Zeolite

Zeolites are naturally abundant aluminosilicate minerals with nanometer scale (0.3-1 nm) 3D open crystalline structures. The channels and cavities of zeolite crystals are made by tetrahedrally coordinated oxy-anions such as SiO_4 and/or AlO_4. The overall zeolite charge depends on the extent of $3^+/5^+$ doping. Pure SiO_2 without any defects is neutral, whereas negative charges appear by replacement of some Si^{4+} atoms by Al^{3+}. Although zeolite can adsorb heavy metal pollutants, zeolite based ceramic membrane has caught considerable attention for water desalination. Estimated global zeolite consumption is 2 Tg/year driving synthetic zeolites production (e.g., zeolite-A produced by Linde Corporation).[69] Mitsui Engineering & Shipbuilding commercializes NaA type zeolite membrane[70] for fractionation of azeotropes (e.g., isopropanol/water, acetonitrile/water and methylethylketone/water) cannot be completely separated by distillation. Therefore, dosing of zeolite into wastewater treatment technology can substantially improve characteristics and quality of treated water by saving on energy and chemical agents.

1.2.10 Other Inorganic Nanoparticles

Numerous other NPs have been examined for water purification technology, such as gold (Au), magnesium oxide (MgO), copper oxide (CuO), manganese oxide (MnO_2), cerium oxide (CeO_2), ZrO_2, and others.[71] Similar to the predominant NPs, they have been used either alone or as component of various composites for adsorption, catalysis, and disinfection processes. Au NP is relatively expensive (US $400/g, US Research NM Inc.), but has physicochemical attributes and optoelectronic properties for chemical and biological senors[72] and catalysis.[73] MgO is a low cost NP for inorganic metal ion adsorption and as an antimicrobial agent.[71] CuO is often used for ground water remediation (mainly As)[74] and has antimicrobial activity. MnO_2 has long been used as a disinfectant[75] as well as advanced oxidation processes (AOP)[76]. CeO_2 has the potential for inorganic metal removal either as individually or associated with ZrO_2 and MnO_2.[71] ISOLUX® Media patented ZrO_2-basted technology for inorganic metal pollutants removal.[77] Therefore, these inorganic NPs have reputation for the production of high quality water through either sigle method or multiple processes where they have hosted water pollutants.

1.3 Organic Nano Polymers

A wide range of polymers, e.g., homopolymer, copolymer and terpolymers used for wastewater treatment since 1950s. Consequently, significant advances of wastewater treatment using nano polymers have been noticed. Nano dendrimer and nano cellulose are commonly studied nano polymers for adsorption process, whereas polymeric protein e.g., aquaporin (AQP) is popular for separation technology. In addition, polymer nanocomposite where NPs doped onto polymer or copolymer matrix have substantially been studied for multi-pollutants wastewater treatment.

1.3.1 Nano Dendrimer

Dendrimers are a soft and highly branched macromolecular NM. Vögtle and co-workers[78] first synthesized dendrimers for trapping smaller molecules in 1978, and are now produced via convergent and divergent grafting methods.[79] A dendrimer has three distinct regions (Fig. S2): a) central hydrophobic core, b) interior cells or voids, and c) external branches coated with a specific functional group such as hydroxyl, epoxy, epoxide, or amine. The size of polymer depends on number and length of the branches attached to the core. The branching units are anchored in a layer-by-layer (LBL) fashion called 'generation' (G). By controlling the assembly process, one can tune dendrimer size, rigidity, hydrophobicity, and hydrophilicity, void, volume and with stimuli response change in solvent polarity, pH, and temperature.[80] Dendrimers are mostly used for specific pollutant adsorption where the functional group is targeted toward a specific pollutant. The company Starpharma marketed poly (esteramine), poly-amidoamine (PAMAM), polypropyleneimine and poly-L-lysine as Priostar®, Starburst®, Astramol® and Polylysine, respectively for both lab experimental and field applications.[81-84] In summary, dendrimers can be engineered with optimized potency that might bring a new platform for controlled water pollutants removal.

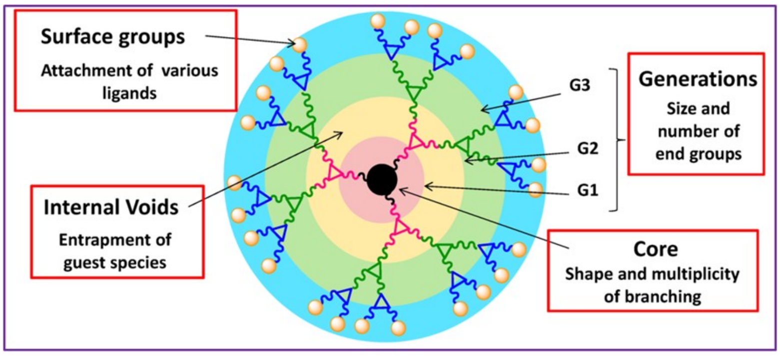

Fig. S2. General structure showing components of a dendrimer. Reprinted with permission from ref.[85] Copyright 2015 Molecular Diversity Preservation International.

1.3.2 Nano cellulose

Nano cellulose is produced in several forms such as cellulose nanocrystals, nanofibrillated cellulose (NFC), and bacterial nano cellulose with all having a fiber morphology that is several µm long and have a diameter between 1 and 100 nm. Nano cellulose is produced by acid and enzymatic catalysis, mechanical hydrolysis, and 2,2,6,6-tetramethylpiperidinyl-1-oxyl (TEMPO)-mediated oxidation.[86] The conversion of cellulose to nano cellulose is important because of increasing SSA and generation of chemically reactive sites or functionalities. Nano cellulose has good mechanical strength (Young's modulus in the range 100–130 GPa)[87] and controlled water solubility. Nano cellulose is a novel biomaterial for water purification, but its utilization in others e.g., papers, cosmetics and medical products (market value of US $47 million in 2014 and projected to approach US $278 million in 2019);[88] reflecting its possibility for commercial water treatment technology.

1.3.3 Biopolymer

Aquaporins (AQPs) are a group of cell membrane spanning proteins that specifically and actively transport water molecules across the cell membrane. The name “aquaporin” was given by Agre et al.[89] who were awarded Nobel Prize in 1993 for discovering the class of proteins. AQP1 was the first discovered and now AQPs 0-12 have been identified in human and mammalian cells.[90] Microbes such as e.g., bacteria, yeast and archaea as well as plants have also been reported to contain AQPs although different than mammalian. A single AQP is roughly 120 kDa and consists of homotetramer structure. AQP have been utilized as a pore channel for desalination membranes. Aquaporin A/S (Copenhagen, Denmark) is the first commercial company who launched Aquaporin Inside™ membrane. In addition, very recently, more than 25 patents have been filed on AQPs-based membrane systems.[91]

2. Asdorption

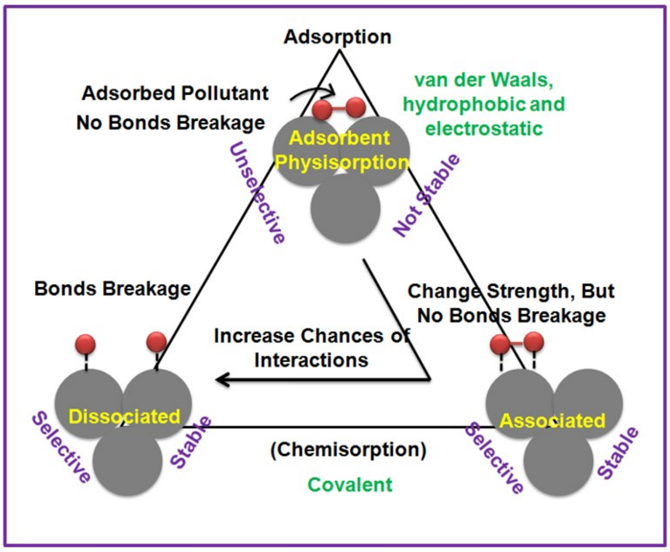

Fig. S3. Schematic representation of the adsorption forces.

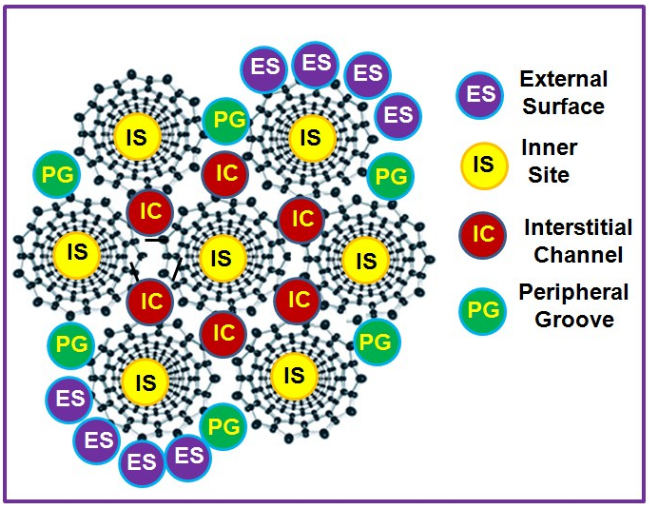

Fig. S4. Structural representation of four predicted major adsorption sites of CNTs in a bundle. Close-ended CNTs: adsorption takes place PG > ES > IC, whereas open-ended CNTs: adsorption proceeds IS of open-ended CNT walls > forms 1D chains in the PG > filling of the remaining axial sites of IC > completion of a quasi-hexagonal monolayer on the ES.

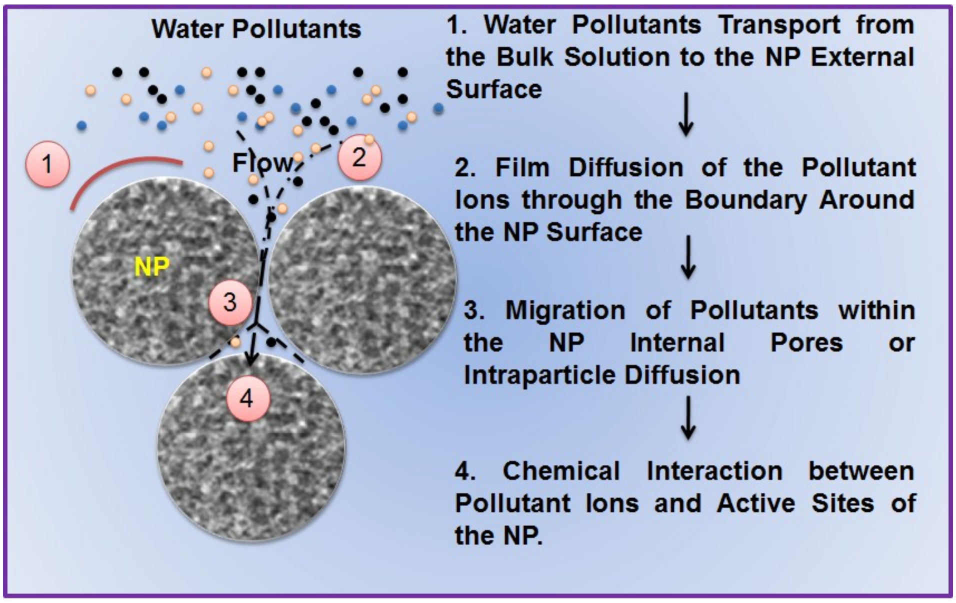

Fig. S5. Mechanism of actions of pollutants adsorption into NPs.

2.1 Isotherms

Figure S6 shows a few adsorption isotherms of turquoise blue QG reactive dye adsorption. Among all the isotherm models (e.g., Langmuir,[92] Freundlich,[93] Halsey,[94] Brunauer–Emmett–Teller (BET),[95] Henderson,[96] Smith,[97] Elovich,[98] and Lagergren[99]), the Langmuir, BET and Freundlich are the most widely used to describe adsorption data. The Langmuir model (equation 1) assumes monolayer adsorption and that all sorption sites have the same binding energy. However, the model does not take into account multilayer adsorption or lateral sorbate-sorbate surface interactions.

$$q = \frac{q_m . K_1 . C}{1 + K_1 . C} \qquad (1)$$

where q, adsorbent concentration (μg/kg); q_m, maximum sorption capacity (μg/kg); K, Langmuir affinity constant (L/mol) and C_w, aqueous concentration (mol/L).

The Freundlich isotherm (equation 2) also assumes monolayer adsorption, but that is for multiple sorption sites with different binding energies.

$$q_e = K_F C_e^{1/n} \qquad (2)$$

where q_e, the amount of adsorbate adsorbed per gram of the adsorbent at equilibrium (mg/g); K_F, Freundlich isotherm constant (mg/g) related to adsorption capacity; C_e, the equilibrium concentration of adsorbate (mg/L); n, Freundlich exponent (unit less) related to adsorption intensity.

1/n values indicate the isotherm would be (1/n = 0), favorable (0 <1/n < 1), or unfavorable (1/n>1). For instance, the value of 1/n <1.0 for As(III) and As(V) adsorption on MWCNT-ZrO_2 adsorbent surface indicates a favorable adsorption process.[100] However, Freundlich isotherm is imperical thus physically meaningless giving minimal mechanistic insight. To determine the kinetics of the mass transfer and chemical reaction that control the rate of the sorption process, the pseudo-first and second order kinetic models as described in equations 3 and 4, respectively,[101] yield insight.

$$q_t = q_e\left(1 - \frac{1}{e^{k_1 t}}\right) \qquad (3)$$

$$q_t = \frac{t}{\frac{1}{k_2 q_e^2} + \frac{t}{q_e}} \qquad (4)$$

where q_t, the adsorbate mass adsorbed by a certain adsorbent mass at time t (mg/g); q_e, the equilibrium adsorption amount (mg/g); k_1, the pseudo-first-order rate constant (1/min) and k_2, the pseudo-second-order rate constant (g/mg min^{-1}).

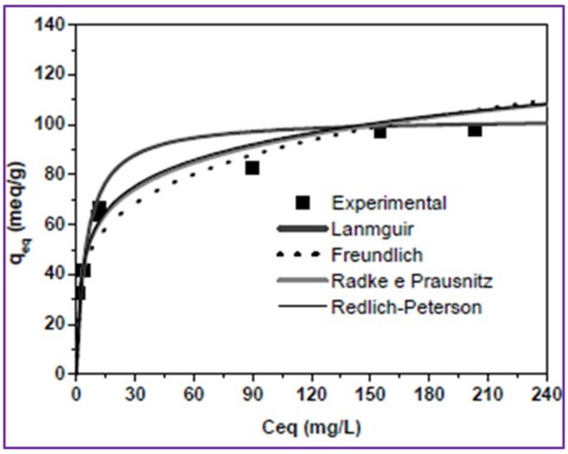

Fig. S6. Schematic representation of a typical batch adsorption of isotherm models. Reprinted with permission from ref.[102] Copyright 2010 SciElo. the Langmuir, Freundlich, Radke-Prausnitz, and Redlich-Peterson isotherm models were fit to the equilibrium data on turquoise blue QG reactive dye adsorption. Among them the Radke-Prausnitz model best represented the equilibrium data for the dye, with coefficients of determination in the range of 0.93 to 0.99[102].

2.2 Reusability of Adsorbents

Rao et al.[103] designed a magnetic MIP using Fe_3O_4 grafted MWCNT, 4-tert-octylphenol, 4-vinyl pyridine, and tetra-ethylorthosilicate as magnetic support, dummy template, functional monomer, and cross-linker, respectively (Fig. S7 (Aa)). The magnetic dummy MIP (mag-DMIPs) was highly selective to 4-nonylphenol, and the MAC was 52.4 mg/g after 20 min contact time. Although the Ms decreases from 40.69 (MWCNT-Fe_3O_4) to 26.52 emu/g (mag-DMIP) because of imprinting polymer, it is still sufficient to separate the adsorbent from solution within 1 min as shown in Fig. S7 (Ab). In order to reusable the mag-DMIP, several washing agents, such as methanol/water, chloroform/water, and acetonitrile/water were evaluated with the methanol/water recovering most of the 4-nonylphenol sorbed to the mag-DMIPs. Electrostatic self-assembly can be used to bind positively charged calcium carbonate ($CaCO_3$) to negatively charged CNT, forming a core-shell structure (Fig. S7 (B)). Increasing adsorption capacity towards 2-naphthol 222 (mg/kg) (Freundlich) and enabling reusability (>90% after four-cycle uses). Assaying an aromatic sorption capacity indicates affinity follows the order of 2-naphthol > naphthalene > 4-chlorophenol.[104] Greater affinity of 2-naphthol is because of its greater hydrophobicity and larger aromatic ring than 4-chlorophenol to the CNT surfaces on the composites. The classical batch sorption experiments, sorbents such as CNT are used as a suspension in a fluiding bed making it difficult to retain the sorbent. One solution is to immobilize the CNT on the membrane or filter to prevent release to the environment. For example, a granular CNT-Al_2O_3 composite[105] is porous and mechanically stable, thus could be used in a practical column sorption application. Wei et al.[106] prepared a granular CNT/Al_2O_3 adsorbent using a hydrothermal calcination process and evaluated potential for removal of pharmaceutical wastewater pollutants such as diclofenac sodium (DS) and carbamazepine (CBZ) as displayed in Fig. S7 (C). Granular CNT/Al_2O_3 had similar adsorption capacity to powder CNT attributed to minimal interference from Al_2O_3, e.g., a CNT/Al_2O_3 reduced CNT agglomeration increasing the SSA from CNT (76) to CNT/Al_2O_3 (237 m^2/g) resulting in a Langmuir CNT/Al_2O_3 MAC of DS (40) and CBZ (60 μmol/L). In order to regenerate the CNT/Al_2O_3, thermal treatment (400°C) was applied to combust the adsorbed DS and CBZ with removal efficiencies of regenerated CNT/Al_2O_3 >60% for both DS and CBZ after ten-cycles. Yang et al.[107] prepared a hollow microsphere using LBL assemblages of sacrificial polystyrene sulfonate (PSS), polycation chitosan (PCHI), and functionalized MWCNT as templates (Fig. S7 (D)). The negatively charged CNT-COO^- binded NH_3^+ of PCHI, such that CNT uniformly wrapped the template surface. PCHI creating a colloid sphere with a large SSA. Few challenges exist for implementing such microspheres for pollutants adsorption. Since the faces of MWCNTs layer (Fig. S7 (D)) were exposed to external milieu of solvents; surface adsorption would be a prominent force rather than internal diffusions depending on spacing between the CNT layers which would call early equilibrium reaction kinetics.

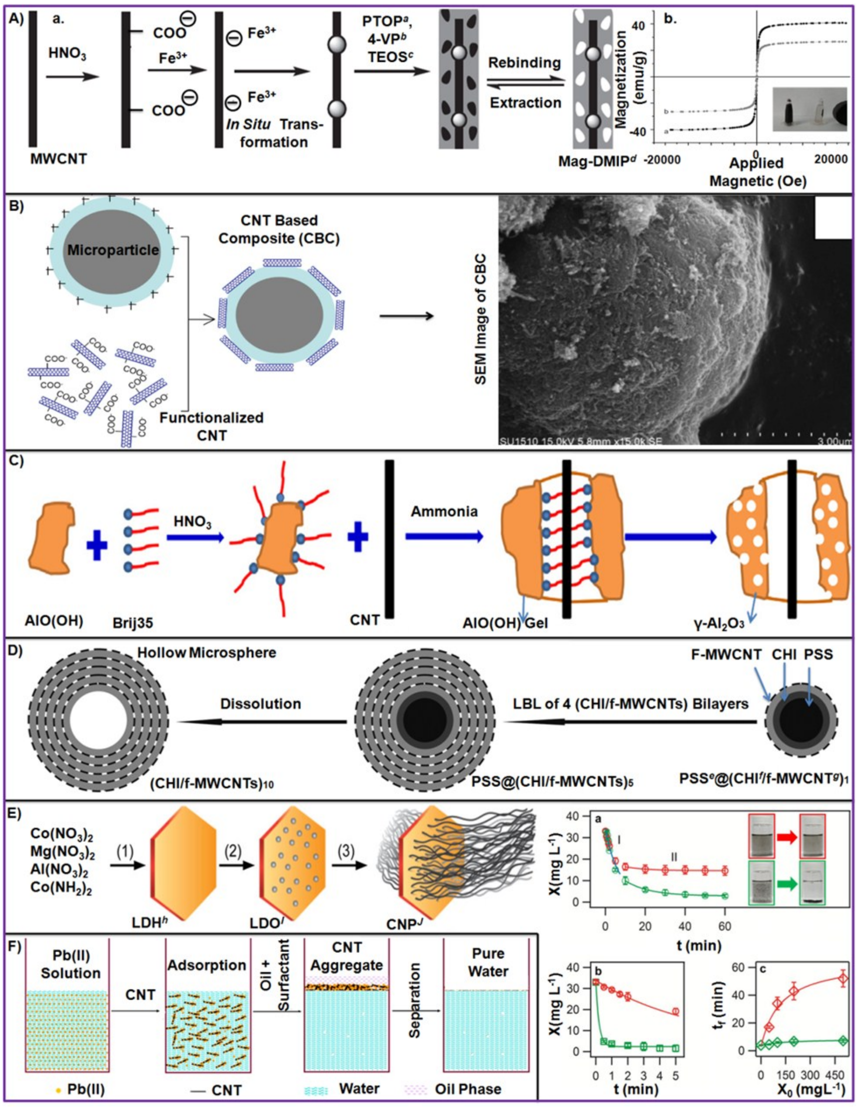

Fig. S7. Recollectable strategies of different CNT adsorbents for water purifications: (A) mag-DMIPs, (B) CNT-based core-shell, (C) granular CNT/Al_2O_3 hybrid, (D) chitosan/CNT LBL assembly, (E) CNPs and (F) CNT/CTAB oil/water interface. Panel A reprinted with permission from ref[103] Copyright 2014 Elsevier. Panel B reprinted with permission from ref.[104] American Chemical Society 2015. Panel C reprinted with permission from ref.[106] Copyright 2013 Elsevier. Panel D reprinted with permission from ref.[107] Copyright 2012 American Chemical Society. Panel E reprinted with permission from ref.[108] Copyright 2012 American Chemical Society. Panel F reprinted with permission from ref.[109] Copyright 2015 Elsevier. Herein [a]4-tert-octylphenol, [b]4-vinyl pyridine, [c]tetra- ethylorthosilicate, [d]magnetic dummy molecularly imprinted polymers, [e]polystyrene sulfonate, [f]chitosan, [g]functionalized MWCNT, [h]layered double hydroxide, [i]layered double oxide, [j]carbon nanotube ponytails.

Recently, Wang et al.[110] prepared a highly reusable CNT ponytail (CNP) by a 3-step process (Fig. S7 (E)). First, Al, Mg, and Co ions were co-precipitated with OH^- and CO_3^{2-} ions to form a layered double hydroxide (LDH) disc. Second, dehydration and decarbonation of LDH was performed to form layered double oxide (LDO) and CoO. At last, CoO was reduced to Co by H_2, and CVD was used to grow CNT the nanometer-thin mineral discs. Diameter, pore sizes and SSA of synthesized CNT were 4-7, 2-100 nm, and 365±10 m^2/g, respectively. The length of CNP was 100 µM and achieved maximum CNT mass and volume fractions. The CNP MB adsorption capacity 150±9 mg/g, (Langmuir) and *Escherichia coli* (*E. coli*) was $2.3 \pm 0.2 \times 10^9$ CFU/g (Langmuir). CNP were separated from solution using three methods: a) sedimentation, b) external magnet, and c) membrane filtration. Sedimentation is very common in both large and small-scale. According to Fig. S7 (Ea), CNP (35 mg/L) settles from the solution and becomes clear within 60 min (colored in green) as compared with free CNT (colored in red). The precipitation followed the following sedimentation model equation 5:

$$X = X_0 e^{-\left(\frac{v}{h}\right)t} \qquad (5)$$

where *X*, changes of carbon concentration on time; *v*, the terminal settling velocity and *h*, the height of the suspension 1.2±0.1 cm.

As shown in Fig. S7 E(a), critical time shift from I to II is displayed by quantitative analyses of changes of *X*. In regime I, both the CNP and CNT precipitate similarly where $X > 15$ mg/L, whereas decreasing *X* is noticed in regime II because of faster CNP precipitation than the free CNT. CNP can also be separated by applying an external magnetic field due to the presence of CoO NP in LDO with an Ms of 1.8 emu/g, which is sufficient to separate >95% of the CNP in <5 min (square) faster than sedimentation (circles) (Fig. S7 (Eb)). Finally, vacuum filtration of 50 mL solution of CNP through 0.8 μm membrane (green) requires less time as compared with CNT (red) (Fig. S7 (Ec)). These results suggest that CNP would be energy and cost efficient adsorbent than the CNT alone. However, since CNP contains highly toxic Co may not be acceptable for water treatment.

Another separation process is to partition CNT at an oil/water (o/w) interface after adsorption as shown in Fig. S7 (F). Cetyltrimethylammonium bromide (CTAB) is used as a CNT surfactant such that the CNT composite coagulates at the (o/w) interface.[109] The composite has a Pb(II) MAC of 259 mg/g at pH 10.5. After adsorption, immiscible cyclohexane added to generate 2 phases attracting all the aqueous phase CNT-Pb(II) through shaking followed by settling. The CNT aggregation allows for easy and recycling.

Fig. S8 displays some most attractive Fe_3O_4-based reusable nanocomposites that have recently been used for water purification. First, Wang et al.[111] used sol-gel process to coat *β*-CD on Fe_3O_4 which adsorbed the polychlorinated biphenyls (PCBs)-28 and 52 (Fig. S8 (a)). The hydrophilic surface and hydrophobic cavity of *β*-CD were responsible to trap the water pollutants with specific sizes.[112] Fe_3O_4@*β*-CD showed higher adsorption capacity of PCB-28 (40.01 mmol/kg) than the PCB-52 (30.32 mmol/kg). Low adsorption of PCB-52 was because of the presence of Cl atoms in phenyl rings which created different steric hindrance effects during adsorption. Although Ms was decreased from 62.13 (Fe_3O_4) to 37.57 emu/g (Fe_3O_4@*β*-CD), it was sufficient to recollect the nanocomposite within 30 sec. Second, in order to adsorb the malachite green, RhB, Hg(II), and Ag(I); polyhedral oligomeric silsesquioxane (POSS) bound with a dithiol organic chain on Fe_3O_4 (Fe_3O_4@POSS-SH) has been studied (Fig. S8 (b)).[113] Fe_3O_4@POSS-SH has shown SSA of 224.20 m^2/g that helps to adsorb 100 and 96% of malachite green and RhB, respectively. On the other hand, the thiol group (-SH) and the POSS sulfur and oxygen atoms have contributed in adsorption of Hg(II) (98.5) and Ag(I) (99.5%) into Fe_3O_4@POSS-SH. The recovered Fe_3O_4@POSS-SH (Ms: 14.29 emu/g) could retain at least 92% of adsorption efficiency after 5-cycle uses, suggesting a good reusability of the nanocomposite. Third, poly(m-phenylenediamine) (PmPD) has been used to coat Fe_3O_4 (Fe_3O_4@PmPD), which increases the Redlich−Peterson MAC of Cr(VI) from 46.79 (Fe_3O_4) to 246.09 mg/g (Fe_3O_4@PmPD) (Fig. S8 (c)).[114] The Cr(VI) removal efficiency of Fe_3O_4@PmPD has found higher than the HA coated Fe_3O_4.[115] Although the adsorption, and reduction of Cr(VI) to Cr(III) have occurred simultaneously in both studies, any chances of increasing the Cr adsorption capacity might be due to the nature and functional groups of polymer used. Washing agent, e.g., NaOH is used to clean Fe_3O_4@PmPD after adsorption and could be recollectable (Ms: 73 emu/g) which retained 70% of the Cr adsorption capacity after 6-cycle uses.

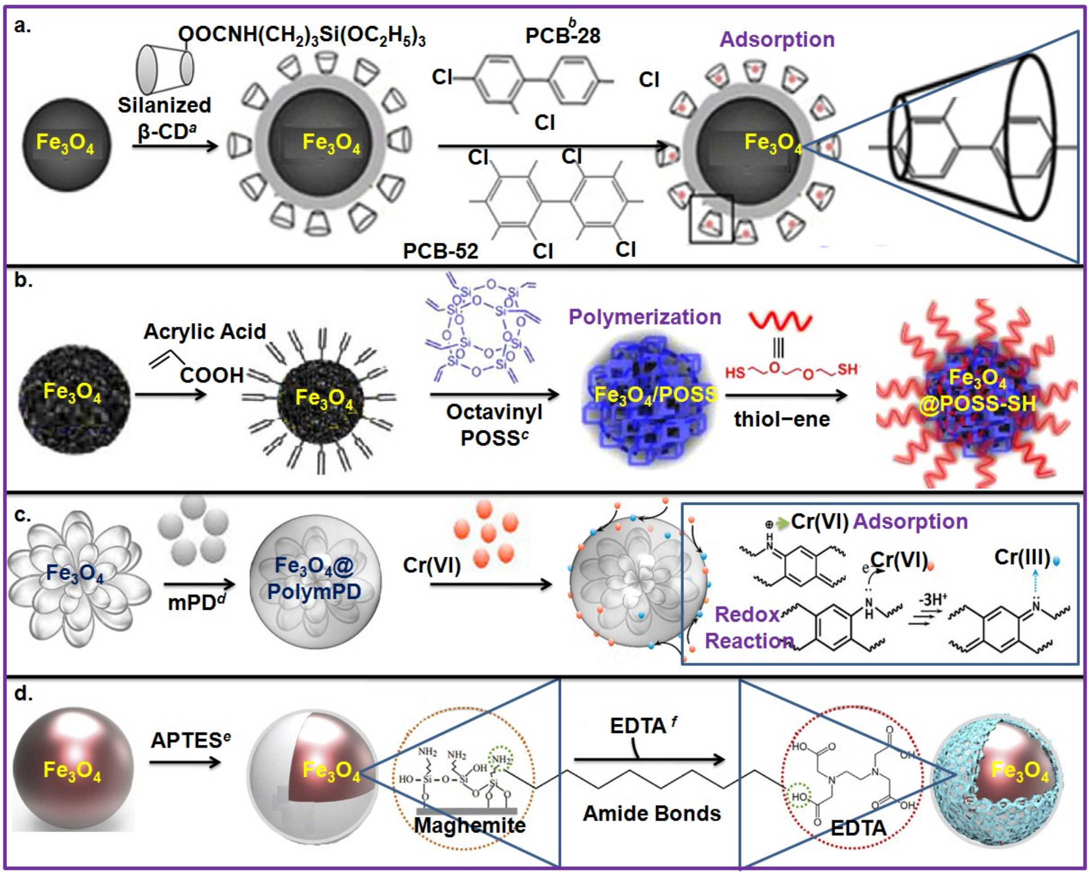

Fig. S8. Fabrications of Fe_3O_4-based reusable nanocomposites and their adsorptive mechanisms: (a) Fe_3O_4@*β*-CD, (b) Fe_3O_4-POSS-SH, (c) Fe_3O_4@PmPD, and (d) Fe_3O_4-EDTA. Panel (a) reprinted with permission from ref.[111] Copyright 2015 Elsevier. Panel (b) reprinted with permission from ref.[113] Copyright 2013 American Chemical Society. Panel (c) reprinted with permission from ref.[114] Copyright 2015 American Chemical Society. Panel (d) reprinted with permission from ref.[116] Copyright 2015 Elsevier Here [a]*β*-cyclodextrin, [b]polychlorinated biphenyls, [c]polyhedral oligomeric silsesquioxane, [d]m-phenylenediamine, [e]3-aminopropyltriethoxysilane and [f]ethylenediaminetetraacetic acid.

At last, EDTA is a popular metal chelating agent that has been used to coat Fe_3O_4 (Fig. S8 (d)). The Fe_3O_4-EDTA showed Langmuir MAC of Cd(II) 79.4 mg/g and Freundlich MAC of Pb(II) 100 mg/g.[116] The nanocomposite could be easily recollectable (Ms: 52.8 emu/g) and nearly 80% of removal efficiency could be maintained after 5-cycle uses. The results can also be comparable with thiosalicylhydrazide modified Fe_3O_4 for metal adsorptions where

Langmuir MAC follows the trend of 188.7 Pb(II) > 107.5 Cd(II) > 76.9 Cu(I) > 51.3 Zn(II) > 27.7 mg/g.[117]

2.3 Factors Controlling Adsorption

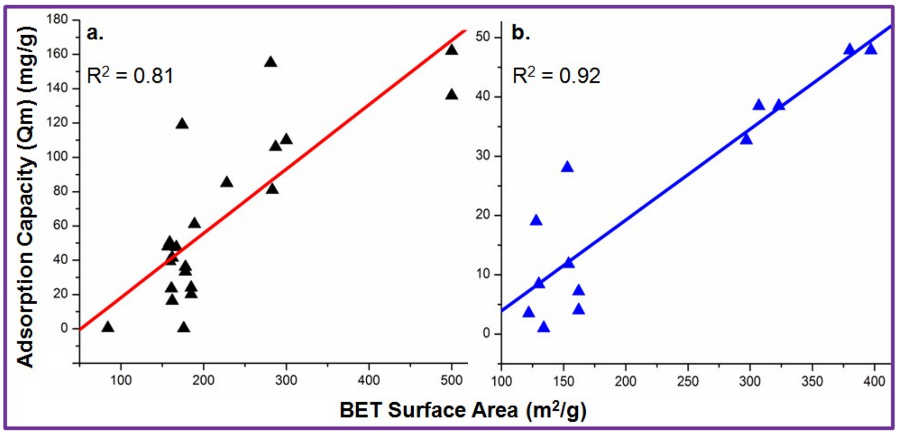

Fig. S9. Relationship between BET surface area of CNT and MAC of (a) organic and (b) inorganic water pollutants. Data collected from refs. (a)[118-130] and refs. (b).[131-138]

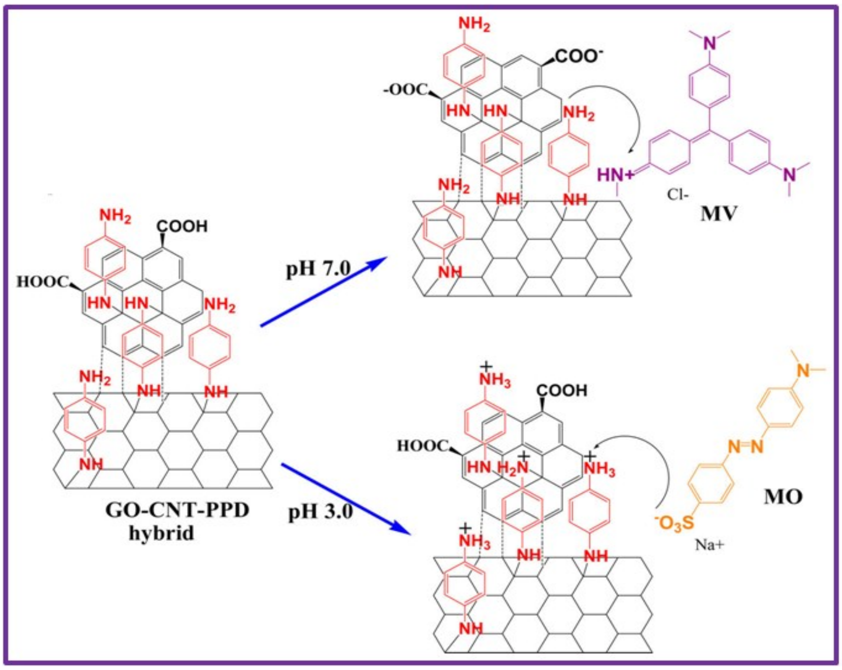

Fig. S10. Selective adsorption of MV and MO into GO-CNT-PPD at pH 7 and 3, respectively. Reprinted with permission from ref.[139] Copyright 2014 American Chemical Society.

3 Catalysis

3.1 Photocatalysis

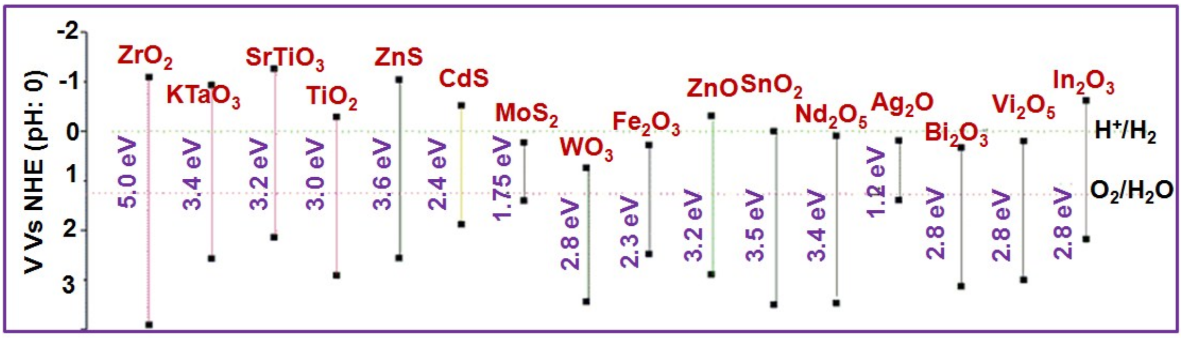

Fig. S11. Band-gaps of some photocatalytic semiconductors. Normal hydrogen electrode (NHE) used as a reference.[140]

Table S1: Photochemistry reactions involved in the photocatalysis with the presence of a semiconductor and organic pollutant (RH).

Reactions	Description
Photoexcitation: semiconductor + hv → e^- + h^+	Upon irradiation of semiconductor (e.g., TiO_2) with light energy equivalent to or greater than its band gap energy (anatase, ~3.2 eV), the electron is excited from VB to the CB. The photonic excitation leaves behind an empty unfilled VB, and thus generates the e^- and h^+
Charge-carrier trapping of e^- : $e^-_{CB} \rightarrow e^-_{TR}$ Here e^-_{CB} means the surface trapped valence band electron and e^-_{TR} represents conduction-band hole	
Charge-carrier trapping of h^+ : $h^+_{VB} \rightarrow h^+_{TR}$	
e -h^+ recombination : $e^-_{TR} + h^+_{VB}(h^+_{TR}) \rightarrow e^-_{CB}$ + heat	In the absence of electron scavengers, the photoexcited e^- recombines with the VB h^+ in nanoseconds with simultaneous dissipation

	of heat energy. Hence, the presence of e^- scavengers is vital for prolonging the recombination and successful functioning of photocatalysis
Oxidation of hydroxyls: $(OH^-)_{ads} + h^+ \rightarrow {}^oOH_{ads}$	Generally, the h^+ reacts with the adsorbed surface OH^- groups on the semiconductor particle to produce surface adsorbed radical ${}^oOH$ads.
Photoexcited e^- scavenging : $(O_2)_{ads} + e^- \rightarrow O_2$	
Protonation of superoxides : $O_2^{-\cdot} + {}^oOH \rightarrow HOO^o$	This O_2^{o-} radical can be further protonated to form the HO_2^o and subsequently H_2O_2
Co-scavenging of e^- : $HOO^o + e^- \rightarrow HO_2^-$	
Formation of H_2O_2: $HOO^- + H^+ \rightarrow H_2O_2$	
Photodegradation by ${}^oOH$: $RH + {}^oOH \rightarrow R^o + H_2O$	Photogenerated h^+ and the formed reactive oxygen species (e.g., ${}^oOH$) can participate in the degradation of organic pollutants
Direct photoholes: $RH + h^+ \rightarrow R^o \rightarrow$ Intermediate(s)/Final Degradation Products	
$RH \xrightarrow{TiO_2/h\nu}$ intermediactes $\rightarrow CO_2 + H_2O +$ inorganic ions	Organic compounds are degraded to their corresponding intermediates and further mineralized to CO_2, H_2O and inorganic ions (from heteroatoms

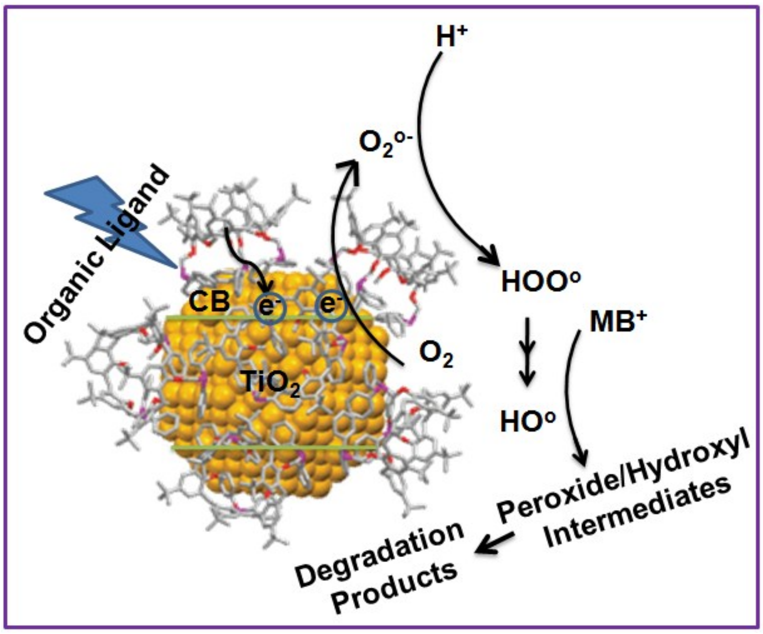

Fig. S12. Mechanisms of the organic-ligand modified TiO_2 for MB degradation under VL irradiation.

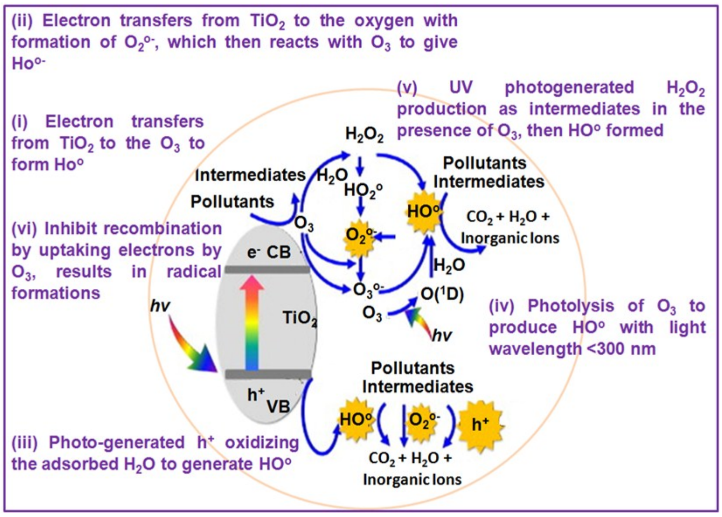

Fig. S13. Summary of photocatalytic ozonations reaction principles. Reprinted with permission from ref.[141] Copyright 2015 Elsevier.

3.2 CWAO

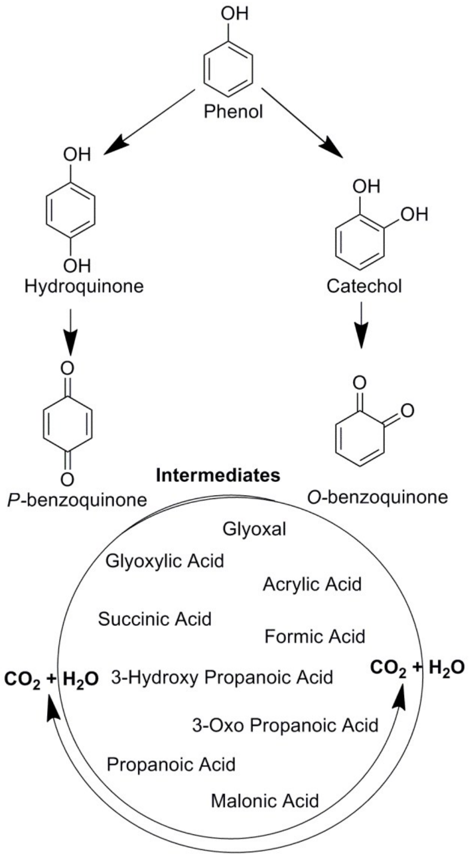

Fig. S14. Simplified reaction pathway for phenol (C)WAO.

3.2.1 CWAO Isotherms

In order to describe the reaction kinetics of (C)WAO, most of the authors have used either the power law[142] or Langmuir-Hinshelwood-Hougen-Watson (LHHW).[143] Although the two models can reasonably explain the reactions of homogenous catalyst, supplementations of different catalysts (e.g., heterogeneous CWAO) follow different reaction orders, which appeal to develop a novel or improved kinetic models (M1-M4) as revealed by Table S2. All the models (M1-M4) fit-well with the experimental data of pure phenol degradation, which has been confirmed from their average absolute relative errors (AARE): 15.7 (M1), 9.7 (M2), 8.9 (M3), and 10.3% (M4);[144] they can be tested for other organic wastewater pollutants degradations.

Table S2. Useful Kinetic Models for Heterogeneous CWAO Reactions

model	equation	comment	refs
M1	$rH = k_1 [A]^p [O_2]^q$ (where rH, heterogeneous combinations and k_1, the surface reaction rate constant)	• an empirical power-law kinetic model • useful for homogeneous or heterogeneous reactions depending on catalyst concentration	[142, 144]
M2	$rH = \dfrac{k_1 K_A K_{O_2} [A][O_2]}{(1 + K_A[A] + K_{O_2}[O_2])^2}$ (K_A and K_{O2}, the pollutant and O_2 adsorption equilibrium constants on catalyst surface, respectively)	• M2 is based on LHHW model • LHHW describes the equilibrium adsorption of pollutant and O_2 into different types of active sites, whereas M2	[143-145]

		represents single-site mechanism and irreversible reaction between them	
M3	$rH = \frac{k_1 K_A K_{O_2}^{0.5}[A][O_2]^{0.5}]}{(1 + K_A[A] + K_{O_2}^{0.5}[O_2]^{0.5})^2}$	• M3 is quite similar to M2 in terms of same active site reaction of pollutant and O_2 molecule, but O_2 molecule undergoes dissociation • surface reaction occurs between the adsorbed pollutant and O_2	144
M4	$rH = \frac{k_1 K_A K_{O_2}^{0.5}[A][O_2]^{0.5}]}{(1 + K_A[A]) + (1 + K_{O_2}^{0.5}[O_2]^{0.5})}$	• suitable for reaction when the dissociated O_2 and pollutant adsorb into distinctly different active sites of the catalyst	144, 146

However, the quality of M1-M4 has been compromised to describe the reactions of CWAO of real wastewater pollutants. Some models have been improved using variables e.g., TOC and COD. Li et al.[147] developed a triangular model called general lumped kinetic model (GLKM) for non-catalytic WAO of acetic acid (Fig. S15 (a)). Since the GLKM model has found unsuitable to express heterogeneous CWAO, Belkacemi et al.[148] further improved the performance of GLKM model based on LHHW called extended lumped kinetic model (ELKM) (Fig. S15 (b)), which could be used to describe the reaction orders of multiple wastewater pollutants degradation. The main difference between these two models is GLKM could not express the adsorption/desorption of reactants/product as compared with ELKM.

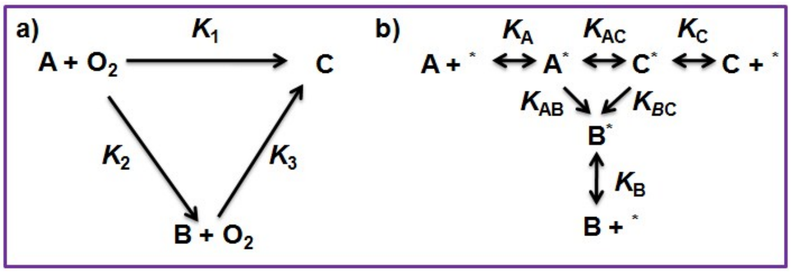

Fig. S15. (a) Reaction orders of GLKM: Lump A, parent compounds and unstable intermediates except acetic acid; Lump B, the refractory intermediates and acetic acid; and Lump C, the end products; (b) Reaction orders of ELKM: Lump A, the parent aqueous compounds adsorbed into catalyst surface; Lump B, the surface reactions of the adsorbed intermediate; and Lump C, the end product. Here *K* and its subscripts represent the kinetic rate constant.

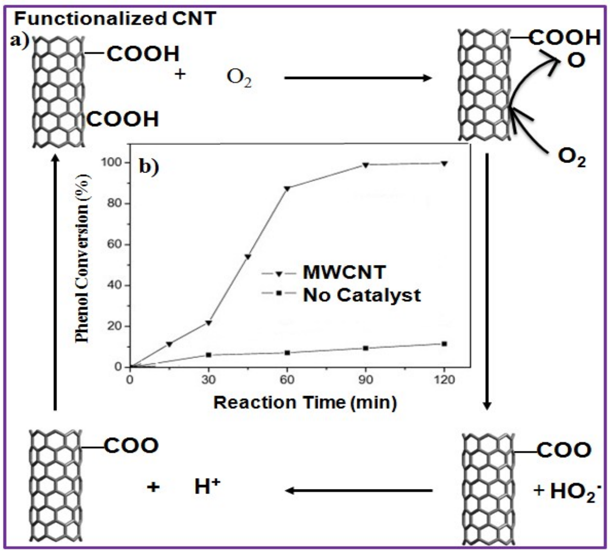

Fig. S16. (a) Mechanism of radical (HO_2^o) formation in CWAO by H_2SO_4/HNO_3 functionalized MWCNT, and (b) efficiency of phenol removal. Reprinted with permission from ref.[149] Copyright 2007 Elsevier.

3.3 Biocatalysis

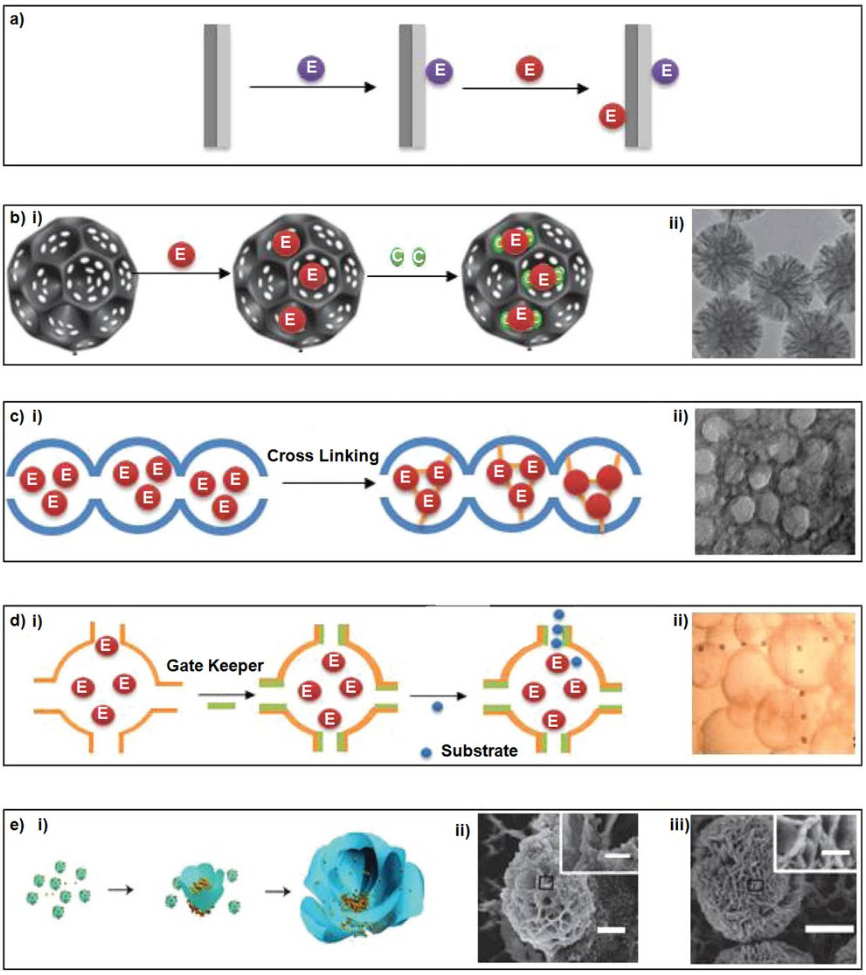

Fig. S17. Selected nanocareers for enzymes immobilization: (a) CNF/CNT favors side-by-side attachments of two enzymes, (b) silica with nanoporous surface architectures is suitable not only to immobilize the enzymes, but also other cofactors and/or biomolecules: i) TEM image of dendrimer like nanoporous silica, (c) ship in a bottle (SB) model: i) to confine enzymes inside the cage and ii) TEM image of SB topology, (d) gate keeper enzyme immobilization for superior substrate diffusion: ii) optical micrograph of nanocages, and (e) protein immobilized onto nanoflower: ii-iii) SEM images of $Cu_3(PO_4)_2.3H_2O$ nanoflowers. Panel (a) reprinted with permission from ref.[150] Copyright 2014 Royal Society. Panel (b) reprinted with permission from ref.[151] Copyright 2013 Wiley-VCH. Panel (c) reprinted with permission from ref.[152] Copyright 2005 Wiley-VCH. Panel (d) reprinted with permission from ref.[153] Copyright 2013 Royal Society of Chemistry. Panel (e) reprinted with permission from ref.[154] Copyright 2012 Nature.

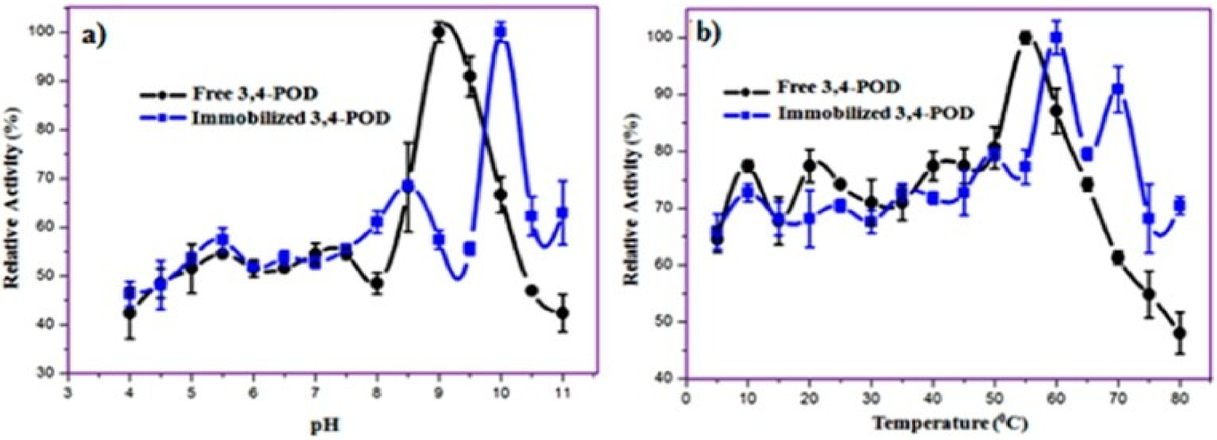

Fig. S18. Effects of (**a**) pH and (**b**) temperature on 3,4-POD activities. Reprinted with permission from ref.[155] Copyright 2016 Nature.

4 Membrane and Filtration

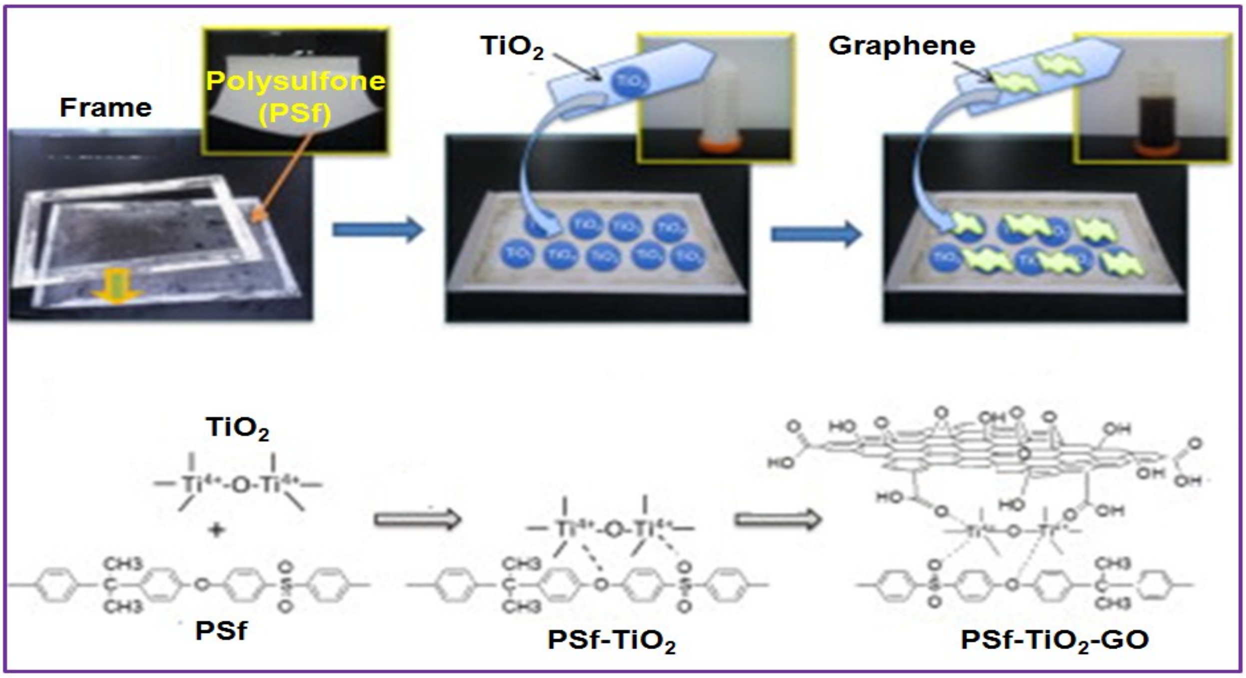

Fig. S19. Illustration of fabrication procedures of TiO_2-GO-PSf composite membrane (top) with their reaction scheme (down). Reprinted with permission from ref.[156] Copyright 2014 Elsevier.

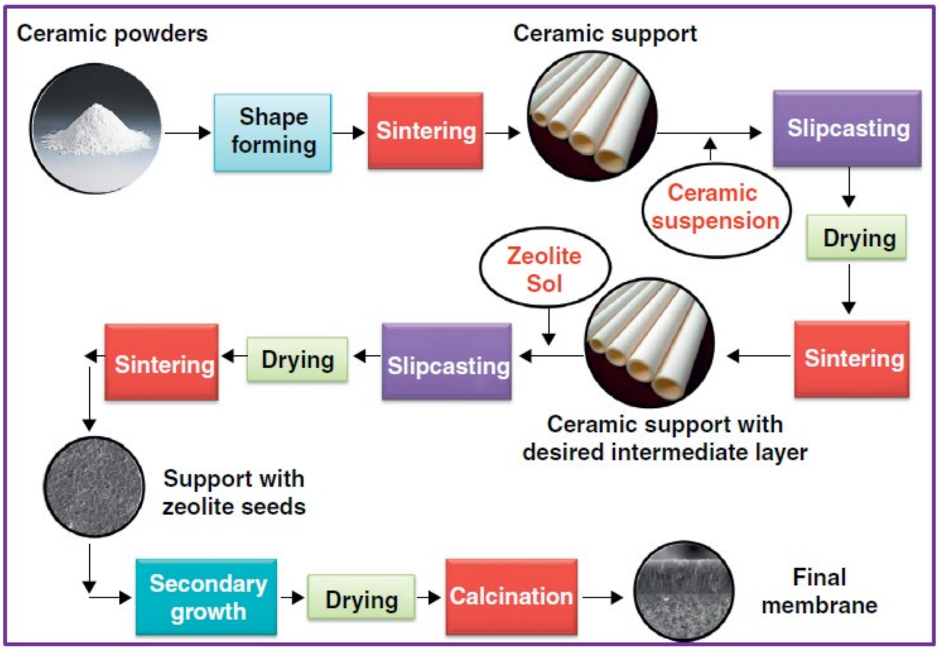

Fig. S20. Secondary growth method to prepare ceramic supported zeolite membrane fabrication. Reprinted with permission from ref.[157] Copyright 2013 Elsevier.

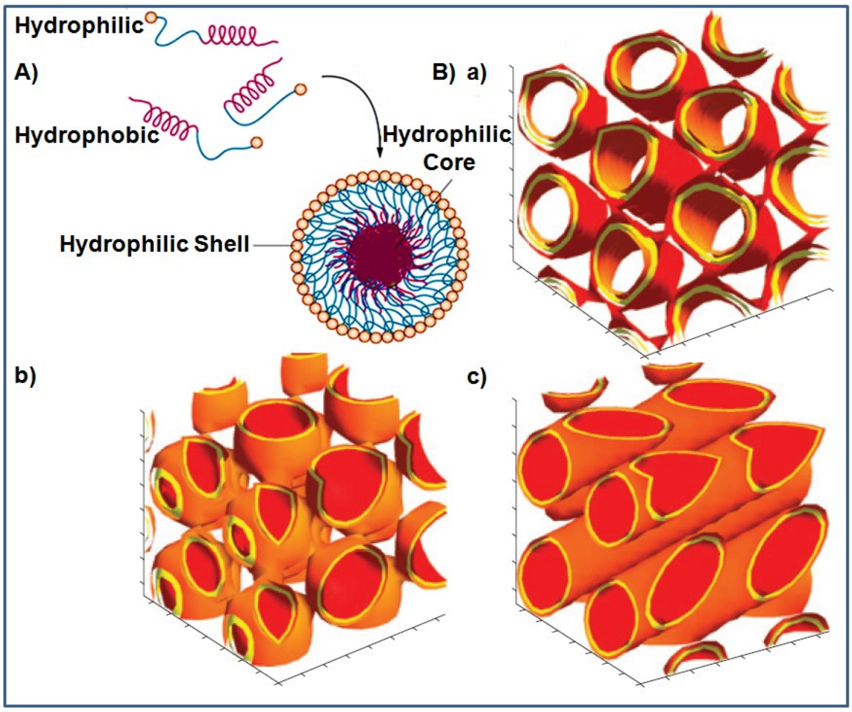

Fig. S21. Schematic illustration of (A) block copolymer, and (B) effects of charge density on the block copolymer phase nanostructures: (a) 2.5% charge, (b) 5.3% charge and (c) 17.0% charge. Panel (A) reprinted with permission from ref.[158] Copyright 2011 Nature. Panel (B) reprinted with permission from ref.[159] Copyright 2014 Nature.

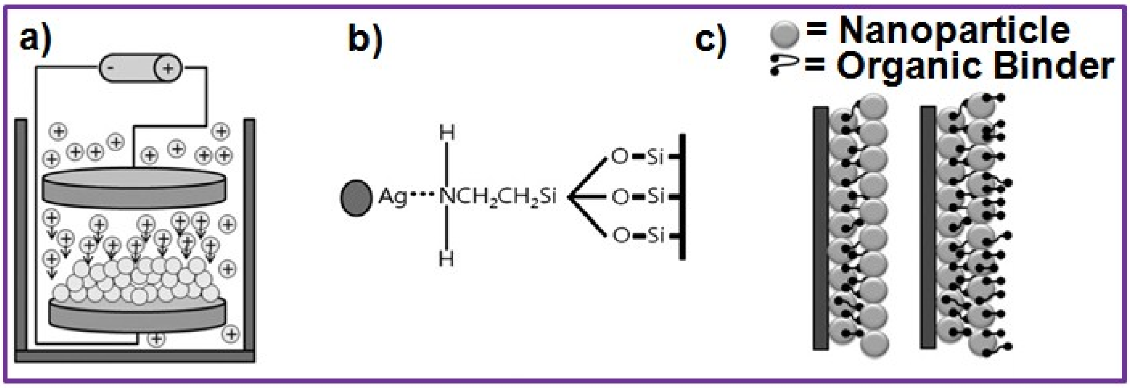

Fig. S22. Illustration of three methods for NP coating onto ceramic membrane: (a) electrophoretic deposition: charged TiO_2 deposits onto alumina, (b) 3-aminopropytriethoxysilane (APTES) molecule as a linker between the Ag NP and the ceramic support, and (c) organic binder (e.g., phytic acid) for doping the Fe_2O_3 NP on ceramic membrane surface using LBL apprach. Reprinted with permission from ref.[160] Copyright 2010 Elsevier.

References

1. R. Das, E. Ali and S. B. Abd Hamid, *Reviews on Advanced Materials Science*, 2014, **38**.
2. V. Georgakilas, J. A. Perman, J. Tucek and R. Zboril, *Chem. Rev.*, 2015.
3. Y. Gogotsi and V. Presser, *Carbon nanomaterials*, CRC Press, 2013.
4. H. W. Kroto, J. R. Heath, S. C. O'Brien, R. F. Curl and R. E. Smalley, *Nature*, 1985, **318**, 162-163.
5. W. Kratschmer, L. D. Lamb, K. Fostiropoulos and D. Huffman, *Nature*, 1990, **347**, 27.
6. H. Singh and M. Srivastava, *Energy sources*, 1995, **17**, 615-640.
7. L. T. Scott, *Angew. Chem. Int. Ed.*, 2004, **43**, 4994-5007.
8. S. Indrawirawan, H. Sun, X. Duan and S. Wang, *Applied Catalysis B: Environmental*, 2015, **179**, 352-362.
9. BCC-Research, The Global Market for Fullerenes, http://www.bccresearch.com/market-research/nanotechnology/NAN034A.html, (accessed 7 June 2016, 2016).
10. J. Brame, Q. Li and P. J. Alvarez, *Trends in Food Science & Technology*, 2011, **22**, 618-624.
11. T. Yadav, 1994.
12. M. Monthioux and V. L. Kuznetsov, *Carbon*, 2006, **44**, 1621-1623.
13. S. Iijima, *nature*, 1991, **354**, 56-58.
14. R. Das, Z. Shahnavaz, M. E. Ali, M. M. Islam and S. B. A. Hamid, *Nanoscale Research Letters*, 2016, **11**, 510.
15. R. Das, S. Bee Abd Hamid, E. Ali, S. Ramakrishna and W. Yongzhi, *Current Nanoscience*, 2015, **11**, 23-35.
16. S. Iijima and T. Ichihashi, *Nature*, 1993, **363**, 603-605.
17. E. W. Wong, P. E. Sheehan and C. M. Lieber, *Science*, 1997, **277**, 1971-1975.
18. S. J. Tans, A. R. M. Verschueren and C. Dekker, *Nature*, 1998, **393**, 49-52.
19. J. Hone, B. Batlogg, Z. Benes, A. T. Johnson and J. E. Fischer, *Science*, 2000, **289**, 1730-1733.
20. M. Ali, R. Das, A. Maamor and S. B. A. Hamid, *Advanced Materials Research*, 2014, **832**, 328-332.
21. R. Das, in *Nanohybrid Catalyst based on Carbon Nanotube*, Springer, 2017, pp. 23-54.
22. D. S. Su, S. Perathoner and G. Centi, *Chem. Rev.*, 2013, **113**, 5782-5816.
23. A. A. Keller, S. McFerran, A. Lazareva and S. Suh, *J. Nanopart. Res.*, 2013, **15**, 1-17.
24. A. S. Adeleye, J. R. Conway, K. Garner, Y. Huang, Y. Su and A. A. Keller, *Chem. Eng. J.*, 2016, **286**, 640-662.
25. A. Ramos, I. Cameán and A. B. García, *Carbon*, 2013, **59**, 2-32.
26. S. Ramakrishna, K. Fujihara, W.-E. Teo, T. Yong, Z. Ma and R. Ramaseshan, *Mater. Today*, 2006, **9**, 40-50.
27. M. Inagaki, Y. Yang and F. Kang, *Adv. Mater.*, 2012, **24**, 2547-2566.
28. A. V. Melechko, V. I. Merkulov, T. E. McKnight, M. A. Guillorn, K. L. Klein, D. H. Lowndes and M. L. Simpson, *J. Appl. Phys.*, 2005, **97**, 041301.
29. A Comparison of Carbon Nanotubes and Carbon Nanofibers, http://pyrografproducts.com/carbon-nanotubes.html, (accessed 6 June 2016, 2016).
30. A. HP Boehm and U. GO Fischer, *Z. Naturforsch., B: Chem. Sci.*, 1962, **17**, 150.
31. K. S. Novoselov, A. K. Geim, S. Morozov, D. Jiang, Y. Zhang, S. a. Dubonos, I. Grigorieva and A. Firsov, *science*, 2004, **306**, 666-669.

32. Y. Hernandez, V. Nicolosi, M. Lotya, F. M. Blighe, Z. Sun, S. De, I. McGovern, B. Holland, M. Byrne and Y. K. Gun'Ko, *Nature nanotechnology*, 2008, **3**, 563-568.
33. W. S. Hummers Jr and R. E. Offeman, *J. Am. Chem. Soc.*, 1958, **80**, 1339-1339.
34. L. Staudenmaier, *Ber Dtsch Chem Ges*, 1898, **31**, 1481-1487.
35. B. Brodie, *Ann. Chim. Phys*, 1855, **45**, 351-353.
36. D. R. Dreyer, S. Park, C. W. Bielawski and R. S. Ruoff, *Chem. Soc. Rev.*, 2010, **39**, 228-240.
37. S. Abdolhosseinzadeh, H. Asgharzadeh and H. S. Kim, *Scientific reports*, 2015, **5**.
38. Y. Zhu, S. Murali, W. Cai, X. Li, J. W. Suk, J. R. Potts and R. S. Ruoff, *Adv. Mater.*, 2010, **22**, 3906-3924.
39. L. Ponomarenko, F. Schedin, M. Katsnelson, R. Yang, E. Hill, K. Novoselov and A. Geim, *Science*, 2008, **320**, 356-358.
40. K. S. Novoselov, V. Fal, L. Colombo, P. Gellert, M. Schwab and K. Kim, *Nature*, 2012, **490**, 192-200.
41. P. Shapira, A. Gök and F. S. Yazdi, *Graphene Research and Enterprise: Mapping Innovation and Business Growth in a Strategic Emerging Technology*, Nesta Working Paper, 2015.
42. T. Pradeep, *Thin Solid Films*, 2009, **517**, 6441-6478.
43. Q. Zhang, Q. Du, M. Hua, T. Jiao, F. Gao and B. Pan, *Environ. Sci. Technol.*, 2013, **47**, 6536-6544.
44. Y. Liu, C. Luo, J. Sun, H. Li, Z. Sun and S. Yan, *Journal of Materials Chemistry A*, 2015, **3**, 5674-5682.
45. I. Ali, *Chem. Rev.*, 2012, **112**, 5073-5091.
46. M. Stefaniuk, P. Oleszczuk and Y. S. Ok, *Chem. Eng. J.*, 2016, **287**, 618-632.
47. L. Li, J. Hu, X. Shi, M. Fan, J. Luo and X. Wei, *Environmental Science and Pollution Research*, 2016, 1-21.
48. W. Yan, H.-L. Lien, B. E. Koel and W.-x. Zhang, *Environmental Science: Processes & Impacts*, 2013, **15**, 63-77.
49. K. M. M. Abou El-Nour, A. a. Eftaiha, A. Al-Warthan and R. A. A. Ammar, *Arabian Journal of Chemistry*, 2010, **3**, 135-140.
50. S. Agnihotri, S. Mukherji and S. Mukherji, *RSC Advances*, 2014, **4**, 3974-3983.
51. V. A. Oyanedel-Craver and J. A. Smith, *Environ. Sci. Technol.*, 2007, **42**, 927-933.
52. U. EPA, *National Center for Environmental Assessment, Office of Research and Development, US Environmental Protection Agency*, 2009, **222**.
53. D. K. Ellsworth, D. Verhulst, T. M. Spitler and B. J. Sabacky, *Chemical innovation*, 2000, **30**, 30-35.
54. X. Yan, T. Ohno, K. Nishijima, R. Abe and B. Ohtani, *Chem. Phys. Lett.*, 2006, **429**, 606-610.
55. M. Pelaez, N. T. Nolan, S. C. Pillai, M. K. Seery, P. Falaras, A. G. Kontos, P. S. Dunlop, J. W. Hamilton, J. A. Byrne and K. O'Shea, *Applied Catalysis B: Environmental*, 2012, **125**, 331-349.
56. A. H. Lu, E. e. L. Salabas and F. Schüth, *Angew. Chem. Int. Ed.*, 2007, **46**, 1222-1244.
57. V. Mameli, A. Musinu, A. Ardu, G. Ennas, D. Peddis, D. Niznansky, C. Sangregorio, C. Innocenti, N. T. Thanh and C. Cannas, *Nanoscale*, 2016, **8**, 10124-10137.
58. I. Gehrke, A. Geiser and A. Somborn-Schulz, *Nanotechnology, science and applications*, 2015, **8**, 1.
59. I. A. Rahman and V. Padavettan, *Journal of Nanomaterials*, 2012, **2012**, 8.
60. C. J. Brinker and G. W. Scherer, *Sol-gel science: the physics and chemistry of sol-gel processing*, Academic press, 2013.
61. Grand-View-Research, Precipitated Silica Market Analysis By Application (Rubber, Agrochemicals, Oral Care, Food Industry)And Segment Forecasts To 2022,

http://www.grandviewresearch.com/industry-analysis/precipitated-silica-market, (accessed 10 June, 2016).
62. S. S. Kumar, P. Venkateswarlu, V. R. Rao and G. N. Rao, *International Nano Letters*, 2013, **3**, 1-6.
63. S. Sabir, M. Arshad and S. K. Chaudhari, *The Scientific World Journal*, 2014, **2014**.
64. Research-&-Market, The Global Market for Zinc Oxide Nanoparticles 2015, http://www.researchandmarkets.com/reports/3293016/the-global-market-for-zinc-oxide-nanoparticles, (accessed 10 June, 2016).
65. L. D. Hart, 1989.
66. A.-I. Moreno-Vega, T. Gomez-Quintero, R.-E. Nunez-Anita, L.-S. Acosta-Torres and V. Castaño, *Journal of Nanotechnology*, 2012, **2012**.
67. P. Patel, *MRS Bull.*, 2014, **39**, 929-929.
68. R. Singh, *Hybrid Membrane Systems for Water Purification: Technology, Systems Design and Operations*, Elsevier, 2006.
69. A. Dyer, 1988.
70. V. Van Hoof, C. Dotremont and A. Buekenhoudt, *Sep. Purif. Technol.*, 2006, **48**, 304-309.
71. K. Simeonidis, S. Mourdikoudis, E. Kaprara, M. Mitrakas and L. Polavarapu, *Environmental Science: Water Research & Technology*, 2016, **2**, 43-70.
72. K. Saha, S. S. Agasti, C. Kim, X. Li and V. M. Rotello, *Chem. Rev.*, 2012, **112**, 2739-2779.
73. B. Puértolas, Á. Mayoral, R. Arenal, B. Solsona, A. Moragues, S. Murcia-Mascaros, P. Amorós, A. B. Hungría, S. H. Taylor and T. García, *ACS Catalysis*, 2015, **5**, 1078-1086.
74. K. J. McDonald, B. Reynolds and K. Reddy, *Scientific reports*, 2015, **5**.
75. S. M. Dizaj, F. Lotfipour, M. Barzegar-Jalali, M. H. Zarrintan and K. Adibkia, *Materials Science and Engineering: C*, 2014, **44**, 278-284.
76. K. A. M. Ahmed, H. Peng, K. Wu and K. Huang, *Chem. Eng. J.*, 2011, **172**, 531-539.
77. ISOLUX®Media, ISOLUX® Media is MEL Chemicals´ patented free-flowing amorphous powder designed specifically for heavy metals reduction in drinking water applications, http://www.zrpure.com/drinking-water/isolux_media.asp, (accessed 11 June, 2016).
78. E. Buhleier, W. Wehner and F. Vögtle, *Chemischer Informationsdienst*, 1978, **9**.
79. D. A. Tomalia, *Prog. Polym. Sci.*, 2005, **30**, 294-324.
80. G. Newkome, C. Moorefield and F. Vögtle, *Dendritic Molecules: Concepts, Syntheses, Perspectives*, 1996, 37-47.
81. D. R. Swanson, B. Huang, H. G. Abdelhady and D. A. Tomalia, *New J. Chem.*, 2007, **31**, 1368-1378.
82. D. A. Tomalia and J. M. Fréchet, *J. Polym. Sci., Part A: Polym. Chem.*, 2002, **40**, 2719-2728.
83. D. Tomalia and M. Rookmaker, *Journal*, 2009.
84. D. Patton, Y. C. Sweeney, T. McCarthy and S. Hillier, *Antimicrob. Agents Chemother.*, 2006, **50**, 1696-1700.
85. A. Sharma and A. Kakkar, *Molecules*, 2015, **20**, 16987-17015.
86. I. A. Sacui, R. C. Nieuwendaal, D. J. Burnett, S. J. Stranick, M. Jorfi, C. Weder, E. J. Foster, R. T. Olsson and J. W. Gilman, *ACS applied materials & interfaces*, 2014, **6**, 6127-6138.
87. A. Dufresne, *Mater. Today*, 2013, **16**, 220-227.
88. BCC-Research, ‘Biomaterial of the Future’ Nanocellulose to Send Market Booming with 42.8% CAGR, http://www.bccresearch.com/pressroom/avm/biomaterial-of-the-

future-nanocellulose-to-send-market-booming-with-42.8-percent-cagr, (accessed 11 June, 2016).

89. P. Agre, S. Sasaki and M. Chrispeels, *American Journal of Physiology-Renal Physiology*, 1993, **265**, F461-F461.
90. C. H. Nielsen, *Analytical and bioanalytical chemistry*, 2009, **395**, 697-718.
91. C. Tang, Z. Wang, I. Petrinić, A. G. Fane and C. Hélix-Nielsen, *Desalination*, 2015, **368**, 89-105.
92. I. Langmuir, *J. Am. Chem. Soc.*, 1918, **40**, 1361-1403.
93. H. Freundlich, *Phys. Chem.*, 1906, **57**, 385-470.
94. G. Halsey, *The Journal of Chemical Physics*, 1948, **16**, 931-937.
95. S. Brunauer, P. H. Emmett and E. Teller, *J. Am. Chem. Soc.*, 1938, **60**, 309-319.
96. A. P. Henderson, L. N. Seetohul, A. K. Dean, P. Russell, S. Pruneanu and Z. Ali, *Langmuir*, 2009, **25**, 931-938.
97. C. Giles, T. MacEwan, S. Nakhwa and D. Smith, *Journal of the Chemical Society (Resumed)*, 1960, 3973-3993.
98. O. G. L. SY Elovich, *zv. Akad. Nauk. SSSR, Otd. Khim. Nauk* 1962, **2**, 209.
99. S. Lagergren, *Band*, 1898, **24**, 1-39.
100. S. A. Ntim and S. Mitra, *J. Colloid Interface Sci.*, 2012, **375**, 154-159.
101. H. Qiu, L. Lv, B.-c. Pan, Q.-j. Zhang, W.-m. Zhang and Q.-x. Zhang, *Journal of Zhejiang University Science A*, 2009, **10**, 716-724.
102. D. Schimmel, K. Fagnani, J. Santos, M. Barros and E. Silva, *Brazilian Journal of Chemical Engineering*, 2010, **27**, 289-298.
103. W. Rao, R. Cai, Y. Yin, F. Long and Z. Zhang, *Talanta*, 2014, **128**, 170-176.
104. L. Xu, J. Li and M. Zhang, *Industrial & Engineering Chemistry Research*, 2015, **54**, 2379-2384.
105. D. Shan, S. Deng, T. Zhao, G. Yu, J. Winglee and M. R. Wiesner, *Chem. Eng. J.*, 2016, **294**, 353-361.
106. H. Wei, S. Deng, Q. Huang, Y. Nie, B. Wang, J. Huang and G. Yu, *Water Res.*, 2013, **47**, 4139-4147.
107. C. Yang and P. Liu, *Industrial & Engineering Chemistry Research*, 2012, **51**, 13346-13353.
108. H. Wang, H. Ma, W. Zheng, D. An and C. Na, *ACS applied materials & interfaces*, 2014.
109. L. Gao, H. Yin, X. Mao, H. Zhu, W. Xiao and D. Wang, *Environmental Science and Pollution Research*, 2015, 1-8.
110. H. Wang, H. Ma, W. Zheng, D. An and C. Na, *ACS applied materials & interfaces*, 2014, **6**, 9426-9434.
111. M. Wang, P. Liu, Y. Wang, D. Zhou, C. Ma, D. Zhang and J. Zhan, *J. Colloid Interface Sci.*, 2015, **447**, 1-7.
112. W. Hu, X. Wu, F. Jiao, W. Yang and Y. Zhou, *Desalination and Water Treatment*, 2016, 1-12.
113. H.-B. He, B. Li, J.-P. Dong, Y.-Y. Lei, T.-L. Wang, Q.-W. Yu, Y.-Q. Feng and Y.-B. Sun, *ACS applied materials & interfaces*, 2013, **5**, 8058-8066.
114. T. Wang, L. Zhang, C. Li, W. Yang, T. Song, C. Tang, Y. Meng, S. Dai, H. Wang and L. Chai, *Environ. Sci. Technol.*, 2015, **49**, 5654-5662.
115. W. Jiang, Q. Cai, W. Xu, M. Yang, Y. Cai, D. D. Dionysiou and K. E. O'Shea, *Environ. Sci. Technol.*, 2014, **48**, 8078-8085.
116. Y. Huang and A. A. Keller, *Water Res.*, 2015, **80**, 159-168.
117. K. Zargoosh, H. Abedini, A. Abdolmaleki and M. R. Molavian, *Industrial & Engineering Chemistry Research*, 2013, **52**, 14944-14954.
118. L. Zhang, P. Fang, L. Yang, J. Zhang and X. Wang, *Langmuir*, 2013, **29**, 3968-3975.

119. X. Yan, B. Shi, J. Lu, C. Feng, D. Wang and H. Tang, *J. Colloid Interface Sci.*, 2008, **321**, 30-38.
120. H.-H. Cho, H. Huang and K. Schwab, *Langmuir*, 2011, **27**, 12960-12967.
121. S. Zhou, Y. Shao, N. Gao, J. Deng and C. Tan, *CLEAN–Soil, Air, Water*, 2013, **41**, 539-547.
122. Y. Lu, M. Jiang, C. Wang, Y. Wang and W. Yang, *Water, Air, & Soil Pollution*, 2013, **224**, 1-12.
123. N. Rambabu, C. A. Guzman, J. Soltan and V. Himabindu, *Chemical Engineering & Technology*, 2012, **35**, 272-280.
124. G.-C. Chen, X.-Q. Shan, Y.-S. Wang, Z.-G. Pei, X.-E. Shen, B. Wen and G. Owens, *Environ. Sci. Technol.*, 2008, **42**, 8297-8302.
125. G.-C. Chen, X.-Q. Shan, Y.-Q. Zhou, X.-e. Shen, H.-L. Huang and S. U. Khan, *J. Hazard. Mater.*, 2009, **169**, 912-918.
126. Q. Fang and B. Chen, *Carbon*, 2012, **50**, 2209-2219.
127. B. Pan, D. Lin, H. Mashayekhi and B. Xing, *Environ. Sci. Technol.*, 2008, **42**, 5480-5485.
128. J. L. Sotelo, A. R. Rodríguez, M. M. Mateos, S. D. Hernández, S. A. Torrellas and J. G. Rodríguez, *Journal of Environmental Science and Health, Part B*, 2012, **47**, 640-652.
129. G.-C. Chen, X.-Q. Shan, Z.-G. Pei, H. Wang, L.-R. Zheng, J. Zhang and Y.-N. Xie, *J. Hazard. Mater.*, 2011, **188**, 156-163.
130. L. A. Al-Khateeb, A. Y. Obaid, N. A. Asiri and M. A. Salam, *Journal of Industrial and Engineering Chemistry*, 2014, **20**, 916-924.
131. Y.-H. Li, S. Wang, J. Wei, X. Zhang, C. Xu, Z. Luan, D. Wu and B. Wei, *Chem. Phys. Lett.*, 2002, **357**, 263-266.
132. R. Q. Long and R. T. Yang, *J. Am. Chem. Soc.*, 2001, **123**, 2058-2059.
133. Y.-H. Li, S. Wang, Z. Luan, J. Ding, C. Xu and D. Wu, *Carbon*, 2003, **41**, 1057-1062.
134. C. Lu and C. Liu, *J. Chem. Technol. Biotechnol.*, 2006, **81**, 1932-1940.
135. H. Wang, A. Zhou, F. Peng, H. Yu and J. Yang, *J. Colloid Interface Sci.*, 2007, **316**, 277-283.
136. H. Wang, A. Zhou, F. Peng, H. Yu and L. Chen, *Materials Science and Engineering: A*, 2007, **466**, 201-206.
137. Y.-H. Li, Z. Di, J. Ding, D. Wu, Z. Luan and Y. Zhu, *Water Res.*, 2005, **39**, 605-609.
138. C. Lu, C. Liu and G. P. Rao, *J. Hazard. Mater.*, 2008, **151**, 239-246.
139. C. Sarkar, C. Bora and S. K. Dolui, *Industrial & Engineering Chemistry Research*, 2014, **53**, 16148-16155.
140. A. Kudo and Y. Miseki, *Chem. Soc. Rev.*, 2009, **38**, 253-278.
141. J. Xiao, Y. Xie and H. Cao, *Chemosphere*, 2015, **121**, 1-17.
142. A. Sadana and J. R. Katzer, *J. Catal.*, 1974, **35**, 140-152.
143. A. Pintar and J. Levec, *Industrial & engineering chemistry research*, 1994, **33**, 3070-3077.
144. J. Guo and M. Al-Dahhan, *Industrial & engineering chemistry research*, 2003, **42**, 5473-5481.
145. S. K. Bhargava, J. Tardio, J. Prasad, K. Föger, D. B. Akolekar and S. C. Grocott, *Industrial & engineering chemistry research*, 2006, **45**, 1221-1258.
146. J. Guo and M. Al-Dahhan, *Industrial & engineering chemistry research*, 2003, **42**, 2450-2460.
147. L. Li, P. Chen and E. F. Gloyna, *AlChE J.*, 1991, **37**, 1687-1697.
148. K. Belkacemi, F. ç. Larachi and A. Sayari, *J. Catal.*, 2000, **193**, 224-237.
149. S. Yang, W. Zhu, X. Li, J. Wang and Y. Zhou, *Catal. Commun.*, 2007, **8**, 2059-2063.

150. M. Misson, H. Zhang and B. Jin, *Journal of the Royal Society Interface*, 2015, **12**, 20140891.
151. X. Du, B. Shi, J. Liang, J. Bi, S. Dai and S. Z. Qiao, *Adv. Mater.*, 2013, **25**, 5981-5985.
152. J. Lee, J. Kim, J. Kim, H. Jia, M. I. Kim, J. H. Kwak, S. Jin, A. Dohnalkova, H. G. Park and H. N. Chang, *Small*, 2005, **1**, 744-753.
153. J. Liu, G. Lan, J. Peng, Y. Li, C. Li and Q. Yang, *Chem. Commun.*, 2013, **49**, 9558-9560.
154. J. Ge, J. Lei and R. N. Zare, *Nature nanotechnology*, 2012, **7**, 428-432.
155. R. Das, S. B. A. Hamid and M. S. M. Annuar, *Scientific Reports*, 2016, **6**, 33572.
156. Y. Gao, M. Hu and B. Mi, *Journal of Membrane Science*, 2014, **455**, 349-356.
157. Y. Lin and M. C. Duke, *Current Opinion in Chemical Engineering*, 2013, **2**, 209-216.
158. H. Shimizu and T. Fujita, *Nature Reviews Nephrology*, 2011, **7**, 407-415.
159. C. E. Sing, J. W. Zwanikken and M. O. de la Cruz, *Nature materials*, 2014, **13**, 694-698.
160. J. Kim and B. Van der Bruggen, *Environ. Pollut.*, 2010, **158**, 2335-2349.